

# Data report: magnetic property studies of sediments and rocks from IODP Expedition 316<sup>1</sup>

Xixi Zhao<sup>2</sup> and Yujin Kitamura<sup>3</sup>

## Chapter contents

<b>Abstract</b> .....	<b>1</b>
<b>Introduction</b> .....	<b>1</b>
<b>Methods and materials</b> .....	<b>3</b>
<b>Results</b> .....	<b>3</b>
<b>Summary</b> .....	<b>4</b>
<b>Acknowledgments</b> .....	<b>5</b>
<b>References</b> .....	<b>5</b>
<b>Figures</b> .....	<b>7</b>
<b>Tables</b> .....	<b>18</b>

## Abstract

In this report, we present paleomagnetic and rock magnetic results from samples recovered during Integrated Ocean Drilling Program Expedition 316. Expedition 316 was designed to evaluate the deformation, inferred depth of detachment, structural partitioning, and fault zone physical characteristics and fluid flow of the Nankai Trough seismogenic zone in the Philippine Sea, off the east coast of southwestern Japan. Drilling was conducted at two sites in the megasplay region (Sites C0004 and C0008) and two sites within the frontal thrust region (Sites C0006 and C0007). Progressive demagnetization experiments conducted on discrete rock samples demonstrate that these rocks contain a stable natural remanent magnetization of both polarities, with unblocking temperatures slightly below the Curie temperature of magnetite. Two general types of behavior were found in the rock magnetic measurements of Expedition 316 cores. One group has a single phase of Ti-poor titanomagnetite. Several representative samples of this titanomagnetite group exhibit a Verwey transition in the vicinity of 120 K, which is in good agreement with the thermomagnetic characteristics of titanomagnetites with Curie temperatures of ~580°C that were identified. The second group is characterized by more than one Curie temperature, which suggests the presence of multiple magnetic phases. Thermomagnetic signatures indicate the inversion of titanomaghemite to a strongly magnetized magnetite and hysteresis ratios clustering toward the multidomain region (with higher  $H_c/H_c$  ratios). The samples analyzed in this study indicate that rock samples from Expedition 316 sites have general good magnetic stability, supporting the inference that the characteristic directions of magnetization isolated from the Nankai Trough drill sites were acquired during original deposition and the stable inclinations identified from these samples are useful for tectonic studies.

## Introduction

The Nankai Trough is formed by subduction of the Philippine Sea plate to the northwest beneath the Eurasian plate (Fig. F1). Here the plate motion of the Philippine Sea plate relative to southwest Japan is commonly quoted as ~4 cm/y, but the rate may be as high as 6.5 cm/y (Seno et al., 1993; Miyazaki and Heki, 2001). The convergence direction is approximately normal to the trench, and sediments of the Shikoku Basin are actively accreting at the defor-

<sup>1</sup>Zhao, X., and Kitamura, Y., 2011. Data report: magnetic property studies of sediments and rocks from IODP Expedition 316. In Kinoshita, M., Tobin, H., Ashi, J., Kimura, G., Lallement, S., Screamton, E.J., Curewitz, D., Masago, H., Moe, K.T., and the Expedition 314/315/316 Scientists, *Proc. IODP*, 314/315/316: Washington, DC (Integrated Ocean Drilling Program Management International, Inc.). doi:10.2204/iodp.proc.314315316.215.2011

<sup>2</sup>Center for the Study of Imaging and Dynamics of the Earth, Institute of Geophysics and Planetary Physics, University of California, Santa Cruz CA 95064, USA. [xzhao@ucsc.edu](mailto:xzhao@ucsc.edu)

<sup>3</sup>Institute for Research on Earth Evolution, Japan Agency for Marine-Earth Science and Technology, 2-15 Natsushima-cho, Yokosuka, Kanagawa 237-0061, Japan.



mation front (Kimura et al., 2007). Integrated Ocean Drilling Program (IODP) Expedition 316 is part of the Nankai Trough Seismogenic Zone Experiment (NanTroSEIZE) complex drilling project. The fundamental goal of NanTroSEIZE is to sample and instrument the plate boundary system at several locations offshore the Kii Peninsula of southwest Japan, where violent, large-scale earthquakes have occurred repeatedly throughout history (Ando, 1975; Tobin and Kinoshita, 2006a, 2006b). The last major earthquakes in this region occurred in 1944 and 1946 (Fig. F1), and the next earthquake is anticipated in the middle of this century.

During Expedition 316, cores were collected from four sites along a transect lying almost perpendicular to the Nankai Trough offshore the Kii Peninsula, central/southwestern Japan (Fig. F2). Two major thrust fault systems were sampled at relatively shallow depths: (1) the shallow portion of the megasplay system (Sites C0004 and C0008) and (2) the initial faulting (or frontal thrust) Sites C0006 and C0007.

Drilling at Site C0004, which is located along the slope of the accretionary prism landward of the inferred intersection of the megasplay fault zone with the seafloor (Fig. F3), revealed that sediments consist of slowly deposited marine sediments and redeposited material from further upslope. This redeposited material provides information about past slope failures, which may be related to past megasplay movement, earthquakes, and tsunamigenesis. Cores from the megasplay fault zone record a complex history of deformation based on structural observations and two age reversals suggested by nannofossil evidence (Kimura et al., 2008). Our postexpedition study suggests that splay fault activity varies through time, with alternating high-activity periods during which splay fault thrusting accommodates a large part of the plate convergence (Strasser et al., 2009). This implies periods of overall accretionary prism mechanical stability alternating with periods of prism instability, the forcing factor(s) of which remain to be discovered.

Site C0008 was drilled at the slope basin seaward of the megasplay fault (Fig. F3). This basin records the history of fault movement. In addition, sediment layers within this basin provide a reference for the sediment underthrust beneath Site C0004. A simplified summary of lithostratigraphic units recovered at Sites C0004 and C0008 is shown in Figure F4.

Drilling at Sites C0006 and C0007 examined the frontal thrust region of the Nankai Trough (Fig. F5). At Site C0006, several fault zones within the prism were reached and sampled. At Site C0007, the plate boundary frontal thrust was penetrated and thrust fault material ranging from breccia to fault gouge

was successfully recovered (Kimura et al., 2008). Unlike results of previous drilling on the Nankai margin, porosity data provide no indication of under-compaction beneath thrust faults. Furthermore, pore water geochemistry data lack clear indicators of fluid flow from depth (Kimura et al., 2008). Site C0006 lithostratigraphy consists of three units (Kimura et al., 2008); Site C0007 lithostratigraphy consists of four (Fig. F6). Turbidite deposits below the slope apron units at both Sites C0006 and C0007 were interpreted by the Expedition 316 scientists as trench deposits. Based on our anisotropy of magnetic susceptibility (AMS) results, Kitamura et al. (2010) proposed a new model for the structural evolution at the toe of the prism, with the following elements:

- Underthrusting sediments induce horizontal stress in the lower part of the wedge, which reduces the effective stress and forms a high-pore pressure anomaly and zones of fracture.
- The frontal thrust is bent geometrically and ceases activity in response to an increase of friction that triggers initiation of the next-generation frontal thrust.
- The upper part of the wedge tilts accordingly, resulting in an unstable slope.

During Expedition 316, pass-through magnetometer measurements were taken on all split-core archive sections. In order to isolate the characteristic remanent magnetization (ChRM), cores were subjected to alternating-field (AF) and thermal demagnetization. Several lithologies have very high coercivity (i.e., resistance to demagnetization by alternating fields) and maximum unblocking temperatures (i.e., the temperature at which natural remanence is completely removed by heating and cooling in a zero-field environment) close to 580°C. Other lithologies are dominated by softer magnetization, with unblocking temperatures of 300°–400°C. Stable ChRM components are observed throughout the majority of the recovered cores, following removal of a low-stability drilling-induced remanence. In some cases, however, the ChRM is not resolved. Several intervals in the frontal thrust sites (e.g., 43.00–138.18 mbsf in Hole C0007B) show little drilling-induced overprinting both in natural remanent magnetization (NRM) intensity and directions. The recovered materials have very high NRM intensities. Preliminary shipboard paleomagnetic results suggested that additional and more detailed paleomagnetic and rock magnetic data were needed from shore-based laboratories to interpret the magnetic behavior of Expedition 316 cores.

Here we present new results from such a study, which involves detailed paleomagnetic and rock magnetic measurements on samples from megasplay



system Sites C0004 and C0008 and frontal thrust Sites C0006 and C0007. The magnetic results from this study will help to more fully understand the nature and origin of the remanence carriers, the history of the sedimentation process, and the faulting activities of the Nankai Trough seismogenic zone.

## Methods and materials

The paleomagnetic and rock magnetic data presented in this paper are from measurements performed at the paleomagnetism laboratories at University of California at Santa Cruz (UCSC; USA) and at the Institute for Rock Magnetism of the University of Minnesota (USA). Progressive AF and thermal demagnetization experiments were carried out to identify the magnetic components and investigate the nature of the remanent magnetization. Thermal demagnetization was carried out with a UCSC-built oven with a residual field of ~7 nT. AF demagnetization was performed using the automatic degaussing system built into the 2G Enterprises cryogenic magnetometer. Changes in the intensity and direction of remanent magnetization vectors during demagnetization experiments were analyzed using orthogonal vector end-point projections (Zijderveld, 1967). Magnetic component directions were identified using principal component analysis (Kirschvink, 1980). Data were processed using software developed by Enkin (1994; [gsc.nrcan.gc.ca/sw/paleo\\_e.php](http://gsc.nrcan.gc.ca/sw/paleo_e.php)).

For rock magnetic characterization, samples were subjected to several magnetic measurements. These included

1. Curie temperature determinations using both low and high applied fields (0.05 and 1 T, respectively);
2. Hysteresis loop parameter measurement: saturation magnetization ( $J_s$ ), saturation remanence ( $J_r$ ), coercivity ( $H_c$ ), and remanent coercivity ( $H_{cr}$ ); and
3. Saturation isothermal remanent magnetization as a function of temperature (10–300 K).

Curie temperatures were determined by measurement of low-field magnetic susceptibility or induced moment versus temperature (using both the Kappabridge susceptometer at UCSC and the Princeton MicroMag vibrating sample magnetometer at the University of Minnesota). To avoid oxidation that could lead to chemical alteration, we conducted thermomagnetic analyses in an inert helium or argon atmosphere. We used a graphic method (Grommé et al., 1969) to determine the Curie temperature that uses the intersection of two tangents to the thermomagnetic curve that bounds the Curie temperature. This method is most straightforward when done by hand,

even though it tends to underestimate Curie temperatures with the two other methods presented by Moskowitz (1981) and Tauxe (1998). Hysteresis parameters were determined on a Princeton Measurements corporation Alternating Gradient Force Magnetometer (MicroMag) at UCSC using 50–100 mg rock chips. Low-temperature measurements were made from 10 K to room temperature on 100–300 mg subsamples in a Quantum Design magnetic property measurement system (MPMS) at the University of Minnesota. Samples were given a saturation isothermal remanent magnetization (SIRM) in a steady magnetic field of 2.5 T at room temperature (300 K) and then cooled in a zero field to 10 K; the remanence was measured at 5 K intervals. The sample was then given a SIRM in a field of 2.5 T before warming it to 300 K in zero field while measuring the remanence value every 5 K in sweep measurement fashion. Unlike in high-temperature measurements, there is no risk of oxidation of a sample since it is at low temperature and is not heated.

A total of 606 discrete paleomagnetic samples were used for shore-based magnetic studies. These 2.5 cm cylindrical samples were drilled from the core sections that contained long pieces, generally taken from the least deformed parts. In all cases, the up-hole direction was recorded on the sample with an orientation arrow before removal from the core section. All samples were kept in a low-field environment (field-free room) to prevent viscous remanence acquisition.

## Results

### Paleomagnetism

One of the major experimental requirements in paleomagnetic research is to isolate the ChRM by selective removal of secondary magnetization. AF and thermal demagnetization of discrete samples revealed that samples have two magnetic components, a low-coercivity drilling overprint, which is removed after 10 to 40 mT or 400°C demagnetization, and the ChRM. Several representative examples are shown in Figure F7. It appears that AF demagnetization is more effective than the thermal procedure in isolating the ChRM. Although the amount and coercivity of overprinting varied, most of it seems to be removed with 20–35 mT AF demagnetization for the majority of samples, allowing us to isolate the ChRM direction using principal component analysis on higher field demagnetization steps (Table T1). Inclination values of ChRM are moderate downward or upward, roughly consistent with the expected inclination for the drill sites (expected inclination at drill sites =  $\pm 52^\circ$ ). Thus, sedimentary cores from Nankai



Trough have recorded a stable component of magnetization with both normal and reversed inclinations (Table T1). A number of samples, however, have inclinations that do not resemble the time-averaged geomagnetic field. At several depth intervals in Site C0004, for example, remanent inclinations are consistently shallower ( $\pm 20^\circ$ – $30^\circ$ ). Nevertheless, we note that the negative ChRM inclinations are not randomly distributed throughout the sequence but are confined to certain zones. Thus, the negative inclinations in these core sections lend support to the notion that the ChRM in these core sections may indicate a reversed polarity.

When compared to shipboard data, our results show that there is a discrepancy between mean inclinations calculated using the discrete samples and long-core measurements. Compared with corresponding discrete samples, the steeper inclination values observed in the long-core measurements may be due to an overprint that has not been completely removed.

## Rock magnetism

### Curie temperature determination of samples

Curie temperature determinations of samples from Expedition 316 sites are presented in Table T2. According to Curie temperatures, three different groups can be recognized. Group 1 is characterized by a single ferromagnetic phase with Curie temperatures between  $570^\circ$  and  $590^\circ\text{C}$ , compatible with that of Ti-poor titanomagnetites (five samples in Table T2). The cooling and heating curves are reasonably reversible (Fig. F8A). Group 2 has multiple magnetic phases. The thermomagnetic curves display one magnetic phase with Curie temperatures around  $280^\circ$ – $390^\circ\text{C}$  on heating, most likely titanomaghemite. The second high-Curie temperature phase is observed around  $580^\circ$ – $600^\circ\text{C}$  (Fig. F8B). The large difference between heating and cooling of the sample suggests a low-temperature oxidized titanomagnetite as the main magnetic mineral. Group 3 also has multiple magnetic phases. The irreversible thermomagnetic curve of this type displays one magnetic phase with Curie temperature  $<200^\circ\text{C}$  on heating (Fig. F8C). The second high Curie temperature phase is observed around  $570^\circ\text{C}$  (five samples in Table T2).

Comparison of the two Curie temperatures (obtained by low-field continuous susceptibility and high-field magnetic moment versus temperature runs) on Sample 316-C0004D-30R-1, 124–126 cm (Table T2), reveals that Curie temperatures determined by susceptibility as a function of temperature are less than those determined by high-field magnetic moment runs (Table T2). It is not clear whether this is due to

nonhomogeneous subsamples used in the two instruments.

### Hysteresis loop parameters

Samples analyzed in this study indicate that rock samples from Expedition 316 sites show a predominance of multidomain domain size (Table T2). Only a few samples exhibit pseudosingle domain size, probably indicating a mixture of multidomain and a significant amount of single-domain grains. The low values of  $J_r/J_s$  in Table T2 probably indicate the presence of ultra-small superparamagnetic grains as well as large multidomain grains (Dunlop and Özdemir (1997)). We plotted examples of a room-temperature hysteresis loop for representative samples that exhibit pseudosingle domain and multidomain behavior (Fig. F9). Hysteresis experiments also indicate both diamagnetic and paramagnetic influence.

### Low-temperature properties

The study of low-temperature phase transition in magnetic minerals has been increasingly utilized in rock magnetism (Banerjee, 1992; Moskowitz et al., 1998; Özdemir et al., 1993, 2002; Cui et al., 1994; Kosterov, 2001a, 2001b, 2002; Smirnov and Tarduno, 2002). Low-temperature measurements were made on representative samples to help characterize magnetic minerals and understand their rock magnetic properties. As shown in Figure F10, the low-temperature curves of SIRM both in zero-field warming and cooling display a variety of features. These include an unblocking temperature in the vicinity of 40–50 K, most likely caused by superparamagnetic magnetite particles (Moskowitz et al., 1993), and a decrease in remanence in the 100–120 K range (Fig. F10), most likely caused by the Verwey transition (Verwey et al., 1947). Figure F10B shows cooling and warming curves for Sample 316-C0006E-44X-6W, 24–26 cm, which has multidomain grain size. Remanence is lost at  $\sim 120$ – $130$  K as the sample both cools and warms through the Verwey transition. On the other hand, no obvious Verwey transition is observed for Sample 316-C0004D-28R-3W, 7–9 cm, during cooling to 10 K. Upon warming from 10 K, however, a tiny bend in remanence occurs near 120 K (Fig. F10D). According to Moskowitz et al. (1998), titanomagnetites with a high Ti replacement level ( $x > 0.04$ ) could not exhibit the Verwey temperature.

## Summary

In summary, sedimentary cores recovered from Expedition 316 drill sites appear to record a stable component of magnetization with both normal and re-

versed inclinations after removal of the pervasive drilling-induced remagnetization. Comparison between continuous and discrete samples indicates that some of the drilling-induced magnetization may remain in long-core measurements even at the highest AF demagnetization level. Rock magnetic data on Expedition 316 samples clearly indicate that titanomagnetite is the dominant mineral and the primary remanence carrier. Several representative samples of this titanomagnetite group exhibit a Verwey transition in the vicinity of 120 K, which is in good agreement with the thermomagnetic characteristics of titanomagnetites with Curie temperatures of ~580°C that were identified. The general good magnetic stability and other properties exhibited by these rocks support the inference that the characteristic directions of magnetization isolated from the Nankai Trough drill sites were acquired during original deposition. The stable inclinations identified from these samples are therefore useful for future tectonic studies.

## Acknowledgments

This research was conducted with samples and data from the Integrated Ocean Drilling Program, an international marine research program dedicated to advancing scientific understanding of the Earth, the deep biosphere, climate change, and Earth processes by sampling and monitoring subseafloor environments. We thank the shipboard scientists, the Marine Works Japan laboratory technicians, and the crews of the D/V *Chikyu* for their help and company during Expedition 316. We also wish to express our appreciation to Dr. Lallan Gupta of IODP and to the shore-based IODP staff for all of their pre- and post-expedition efforts. X. Zhao wants to extend special thanks to the paleomagnetism group of the Institute for Rock Magnetism at the University of Minnesota for their support. Financial support for various parts of this research was provided by grants from the US Science Support Program of the Consortium for Ocean Leadership and National Science Foundation grants EAR 0633891 and 0911331 to X. Zhao. Funding was also provided by the Center for the Study of Imaging and Dynamics of the Earth, Institute of Geophysics and Planetary Physics, at the University of California Santa Cruz, contribution number 507.

## References

- Ando, M., 1975. Source mechanisms and tectonic significance of historical earthquakes along the Nankai Trough, Japan. *Tectonophysics*, 27(2):119–140. doi:[10.1016/0040-1951\(75\)90102-X](https://doi.org/10.1016/0040-1951(75)90102-X)
- Banerjee, S.K., 1992. Applied rock magnetism in the 1990's: potential breakthrough in a new user-driven science. *Eos, Trans. Am. Geophys. Union*, 73:142–143.
- Cui, Y., Verosub, K.L., and Roberts, A.P., 1994. The effect of low-temperature oxidation on large multi-domain magnetite. *Geophys. Res. Lett.*, 21(9):757–760. doi:[10.1029/94GL00639](https://doi.org/10.1029/94GL00639)
- Dunlop, D.J., and Özdemir, Ö., 1997. *Rock Magnetism: Fundamentals and Frontiers*: Cambridge (Cambridge Univ. Press).
- Dunlop, D. J., 2002. Theory and application of the Day plot ( $M_r/M_s$  versus  $H_{cr}/H_c$ ), 2. Application to data for rocks, sediments, and soils. *J. Geophys. Res.*, 107(B3):2057. doi:[10.1029/2001JB000487](https://doi.org/10.1029/2001JB000487)
- Grommé, C.S., Wright, T.L., and Peck, D.L., 1969. Magnetic properties and oxidation of iron-titanium oxide minerals in Alae and Makaopuhi lava lakes, Hawaii. *J. Geophys. Res., [Solid Earth]*, 74(22):5277–5293. doi:[10.1029/JB074i022p05277](https://doi.org/10.1029/JB074i022p05277)
- Kimura, G., Kitamura, Y., Hashimoto, Y., Yamaguchi, A., Shibata, T., Ujiie, K., and Okamoto, S., 2007. Transition of accretionary wedge structures around the up-dip limit of the seismogenic subduction zone. *Earth Planet. Sci. Lett.*, 225(3–4):471–484. doi:[10.1016/j.epsl.2007.01.005](https://doi.org/10.1016/j.epsl.2007.01.005)
- Kimura, G., Scrceton, E.J., Curewitz, D., and the Expedition 316 Scientists, 2008. NanTroSEIZE Stage 1A: NanTroSEIZE shallow megasplay and frontal thrusts. *IODP Prel. Rept.*, 316. doi:[10.2204/iodp.pr.316.2008](https://doi.org/10.2204/iodp.pr.316.2008)
- Kirschvink, J.L., 1980. The least-squares line and plane and the analysis of palaeomagnetic data. *Geophys. J. R. Astron. Soc.*, 62(3):699–718. doi:[10.1111/j.1365-246X.1980.tb02601.x](https://doi.org/10.1111/j.1365-246X.1980.tb02601.x)
- Kitamura, Y., Kanamatsu, T., and Zhao, X., 2010. Structural evolution in accretionary prism toe revealed by magnetic fabric analysis from IODP NanTroSEIZE Expedition 316. *Earth Planet. Sci. Lett.*, 292(1–2):221–230. doi:[10.1016/j.epsl.2010.01.040](https://doi.org/10.1016/j.epsl.2010.01.040)
- Kosterov, A., 2001a. Magnetic hysteresis of pseudo-single-domain and multidomain magnetite below the Verwey transition. *Earth Planet. Sci. Lett.*, 186(2):245–253. doi:[10.1016/S0012-821X\(01\)00250-3](https://doi.org/10.1016/S0012-821X(01)00250-3)
- Kosterov, A., 2001b. Magnetic properties of subaerial basalts at low temperatures. *Earth, Planets Space*, 53(9):883–892. <http://www.terrapub.co.jp/journals/EPS/pdf/2001/5309/53090883.pdf>
- Kosterov, A., 2002. Low-temperature magnetic hysteresis properties of partially oxidized magnetite. *Geophys. J. Int.*, 149(3):796–804. doi:[10.1046/j.1365-246X.2002.01686.x](https://doi.org/10.1046/j.1365-246X.2002.01686.x)
- Miyazaki, S., and Heki, K., 2001. Crustal velocity field of southwest Japan: subduction and arc-arc collision. *J. Geophys. Res., [Solid Earth]*, 106(B3):4305–4326. doi:[10.1029/2000JB900312](https://doi.org/10.1029/2000JB900312)
- Moskowitz, B.M., 1981. Methods for estimating Curie temperatures of titanomaghemitites from experimental  $J_s$ - $T$  data. *Earth Planet. Sci. Lett.*, 53(1):84–88. doi:[10.1016/0012-821X\(81\)90028-5](https://doi.org/10.1016/0012-821X(81)90028-5)



- Moskowitz, B.M., Frankel, R.B., and Bazylinski, D.A., 1993. Rock magnetic criteria for the detection of biogenic magnetite. *Earth Planet. Sci. Lett.*, 120(3–4):283–300. [doi:10.1016/0012-821X\(93\)90245-5](https://doi.org/10.1016/0012-821X(93)90245-5)
- Moskowitz, B.M., Jackson, M., and Kissel, C., 1998. Low-temperature magnetic behavior of titanomagnetites. *Earth Planet. Sci. Lett.*, 157(3–4):141–149. [doi:10.1016/S0012-821X\(98\)00033-8](https://doi.org/10.1016/S0012-821X(98)00033-8)
- Özdemir, Ö., Dunlop, D.J., and Moskowitz, B.M., 1993. The effect of oxydation on the Verwey transition in magnetite. *Geophys. Res. Lett.*, 20(16):1671–1674. [doi:10.1029/93GL01483](https://doi.org/10.1029/93GL01483)
- Özdemir, Ö., Dunlop, D.J., and Moskowitz, B.M., 2002. Changes in remanence, coercivity, and domain state at low temperature in magnetite. *Earth Planet. Sci. Lett.*, 194(3–4):343–358. [doi:10.1016/S0012-821X\(01\)00562-3](https://doi.org/10.1016/S0012-821X(01)00562-3)
- Seno, T., Stein, S., and Gripp, A.E., 1993. A model for the motion of the Philippine Sea plate consistent with NUVEL-1 and geological data. *J. Geophys. Res., [Solid Earth]*, 98(B10):17941–17948. [doi:10.1029/93JB00782](https://doi.org/10.1029/93JB00782)
- Smirnov, A.V., and Tarduno, J.A., 2002. Magnetic field control of the low-temperature magnetic properties of stoichiometric and cation-deficient magnetite. *Earth Planet. Sci. Lett.*, 194(3–4):359–368. [doi:10.1016/S0012-821X\(01\)00575-1](https://doi.org/10.1016/S0012-821X(01)00575-1)
- Strasser, M., Moore, G.F., Kimura, G., Kitamura, Y., Kopf, A.J., Lallemant, S., Park, J.-O., Screamton, E.J., Su, X., Underwood, M.B., and Zhao, X., 2009. Origin and evolution of a splay fault in the Nankai accretionary wedge. *Nat. Geosci.*, 2(9):648–652. [doi:10.1038/ngeo609](https://doi.org/10.1038/ngeo609)
- Tauxe, L., 1998. *Paleomagnetic Principles and Practice*: Dordrecht, Netherlands (Kluwer Academic Publishers).
- Tobin, H.J., and Kinoshita, M., 2006a. Investigations of seismogenesis at the Nankai Trough, Japan. *IODP Sci. Prosp.*, NanTroSEIZE Stage 1. [doi:10.2204/iodp.sp.nantroseize1.2006](https://doi.org/10.2204/iodp.sp.nantroseize1.2006)
- Tobin, H.J., and Kinoshita, M., 2006b. NanTroSEIZE: the IODP Nankai Trough Seismogenic Zone Experiment. *Sci. Drill.*, 2:23–27. [doi:10.2204/iodp.sd.2.06.2006](https://doi.org/10.2204/iodp.sd.2.06.2006)
- Verwey, E.J., Haayman, P.W., and Romeijn, F.C., 1947. Physical properties and cation arrangements of oxides with spinel structures, II. Electronic conductivity. *J. Chem. Phys.*, 15(4):181–187. [doi:10.1063/1.1746466](https://doi.org/10.1063/1.1746466)
- Zijderveld, J.D.A., 1967. AC demagnetization of rocks: analysis of results. In Collinson, D.W., Creer, K.M., and Runcorn, S.K. (Eds.), *Methods in Palaeomagnetism*: New York (Elsevier), 254–286.

**Initial receipt:** 29 October 2010

**Acceptance:** 28 July 2011

**Publication:** 2 November 2011

**MS 314315316-215**

**Figure F1.** Nankai Trough off southwestern Japan, locus of Philippine Sea plate (PSP) subduction beneath Honshu and Shikoku islands. Yellow arrow = convergence direction between PSP and Japan. Rupture zones of 1944 and 1946 earthquakes are also shown. Stars = epicenter locations for earthquake nucleation. Red dashed line = Kumano Basin drilling area. NAP = North American plate, EP = Eurasian plate, PP = Pacific plate. (After Kimura et al., 2008.)

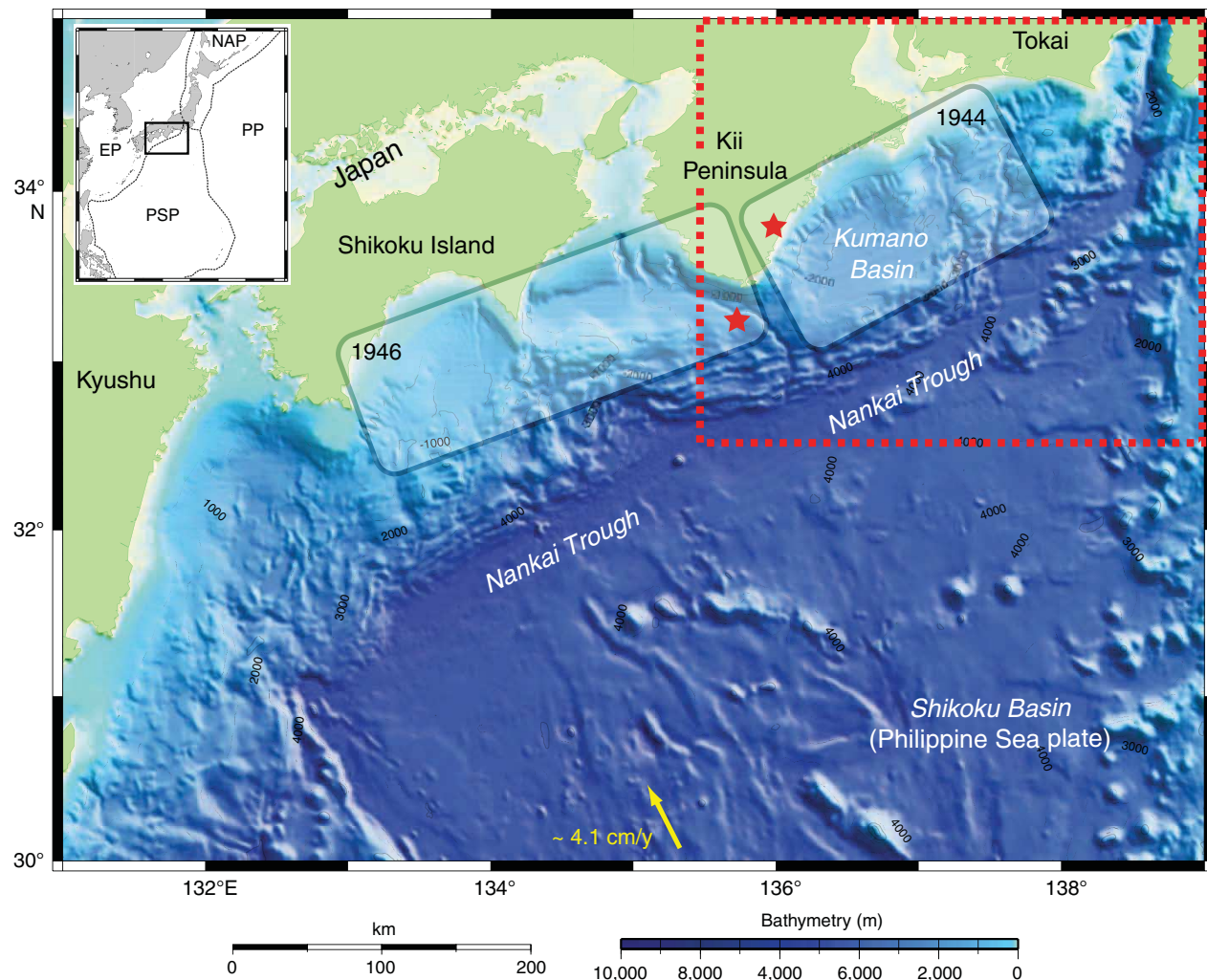


**Figure F2.** Locations of four drilling sites occupied during Expedition 316 (after Kimura et al., 2008). NAP = North American plate, EP = Eurasian plate, PP = Pacific plate, PSP = Philippine Sea plate.

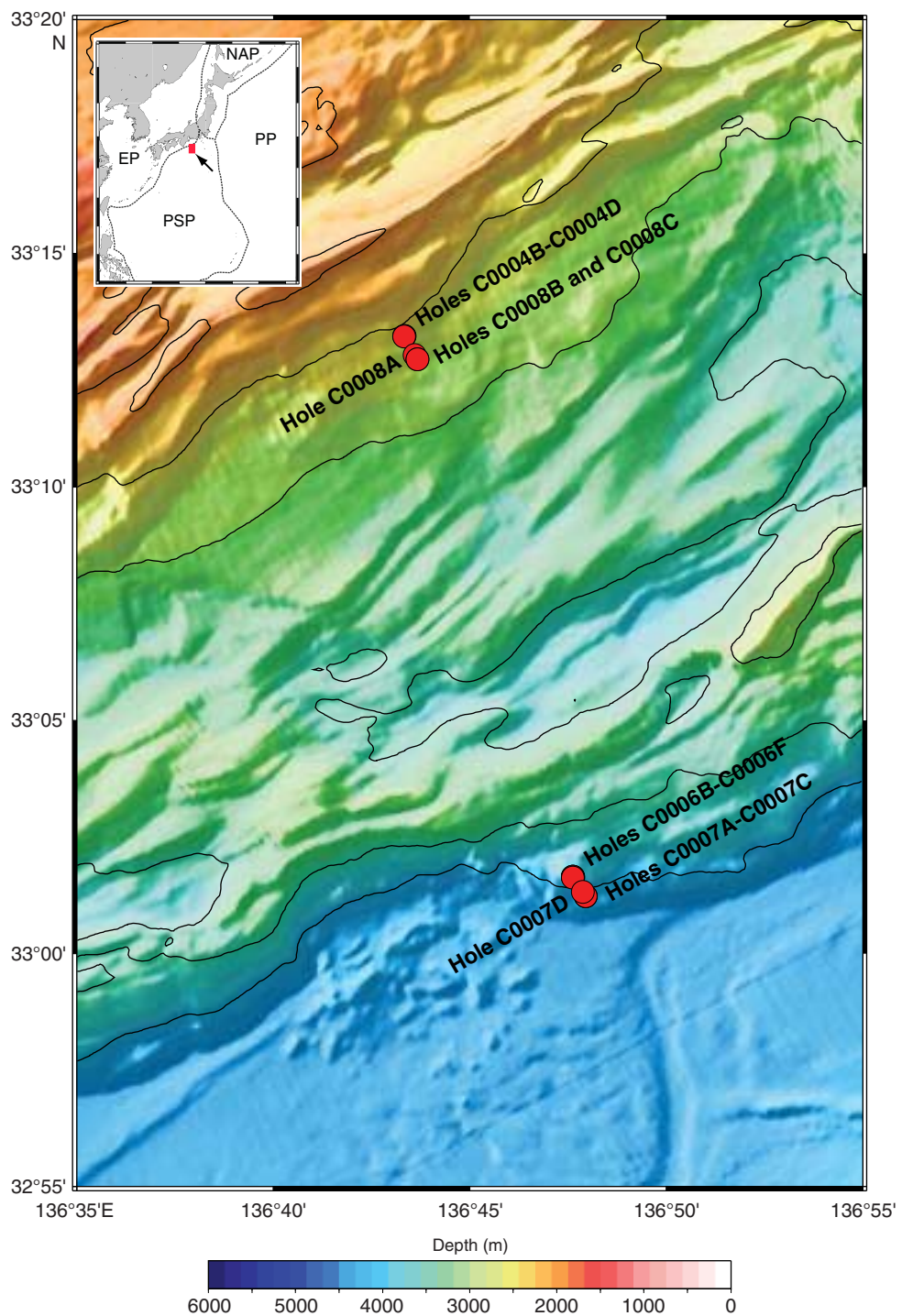
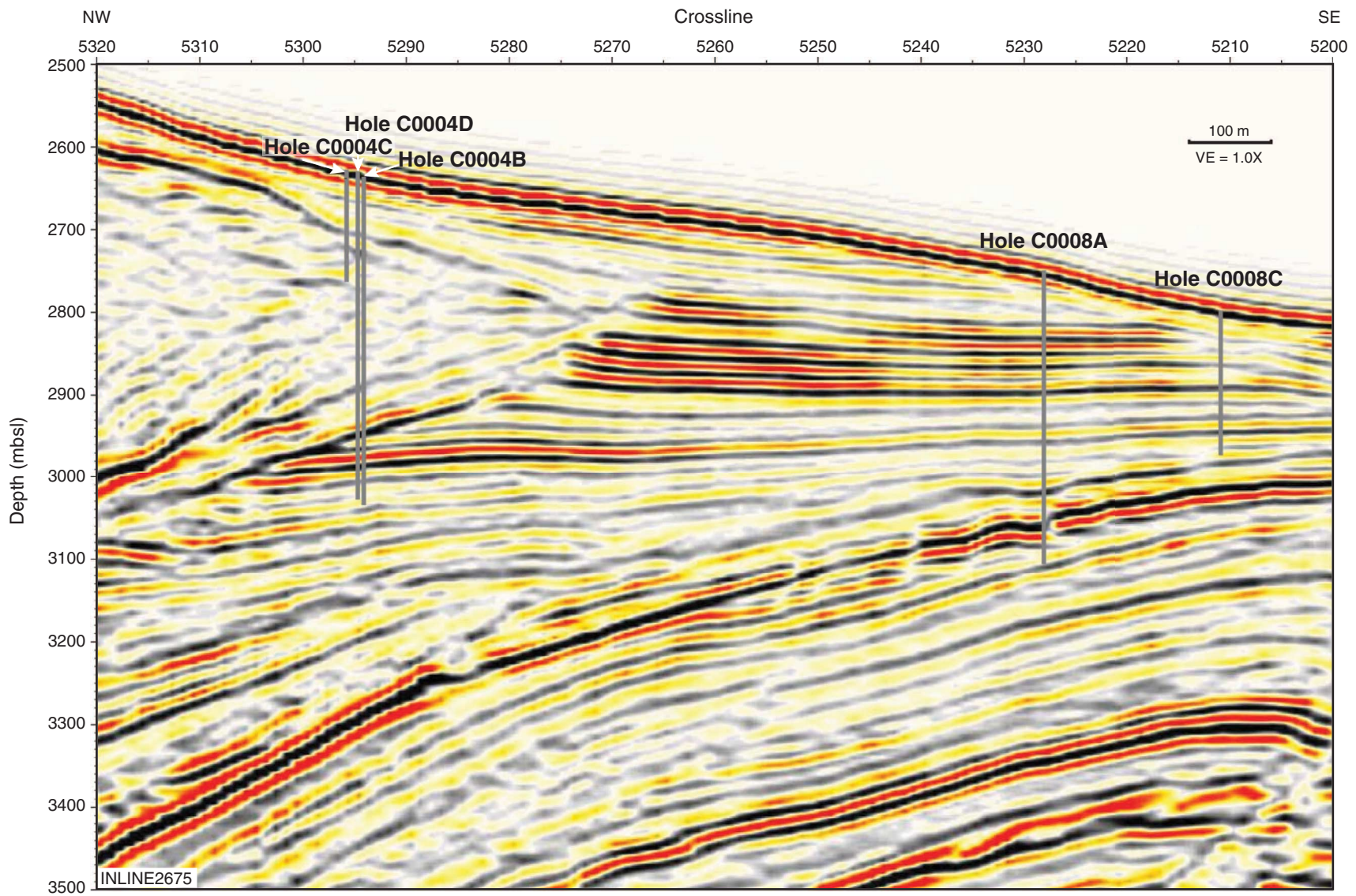


Figure F3. Three-dimensional seismic profile crossing Sites C0004 and C0008 (after Kimura et al., 2008). VE = vertical exaggeration.





**Figure F4.** Summary of lithostratigraphic units for (A) Site C0004 and (B) Site C0008. (Modified from M. Underwood's unpublished “official” stratigraphy columns for Expedition 316 drill sites; [jamstec-cdex.projectpath.com/P17230024/](http://jamstec-cdex.projectpath.com/P17230024/)).

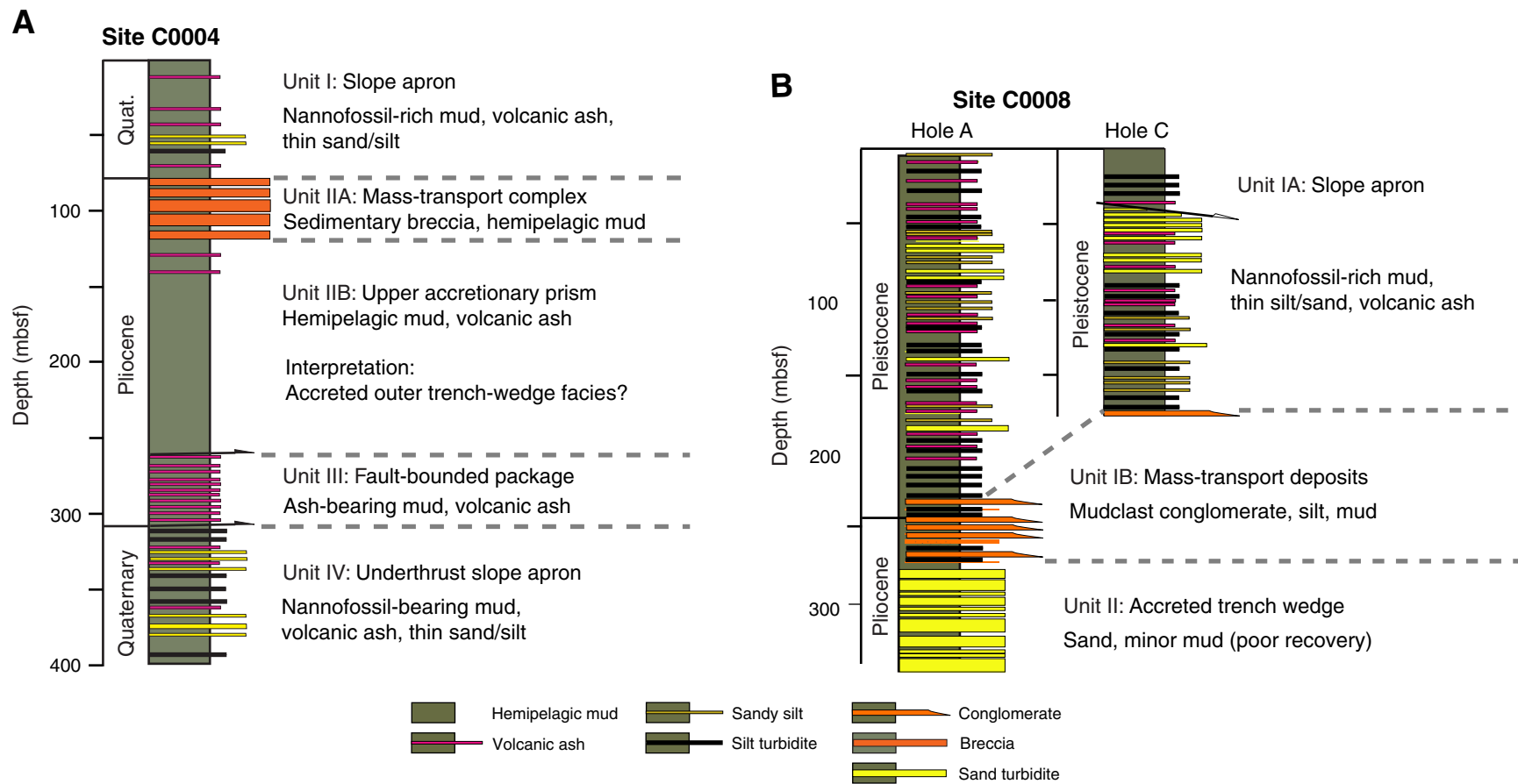
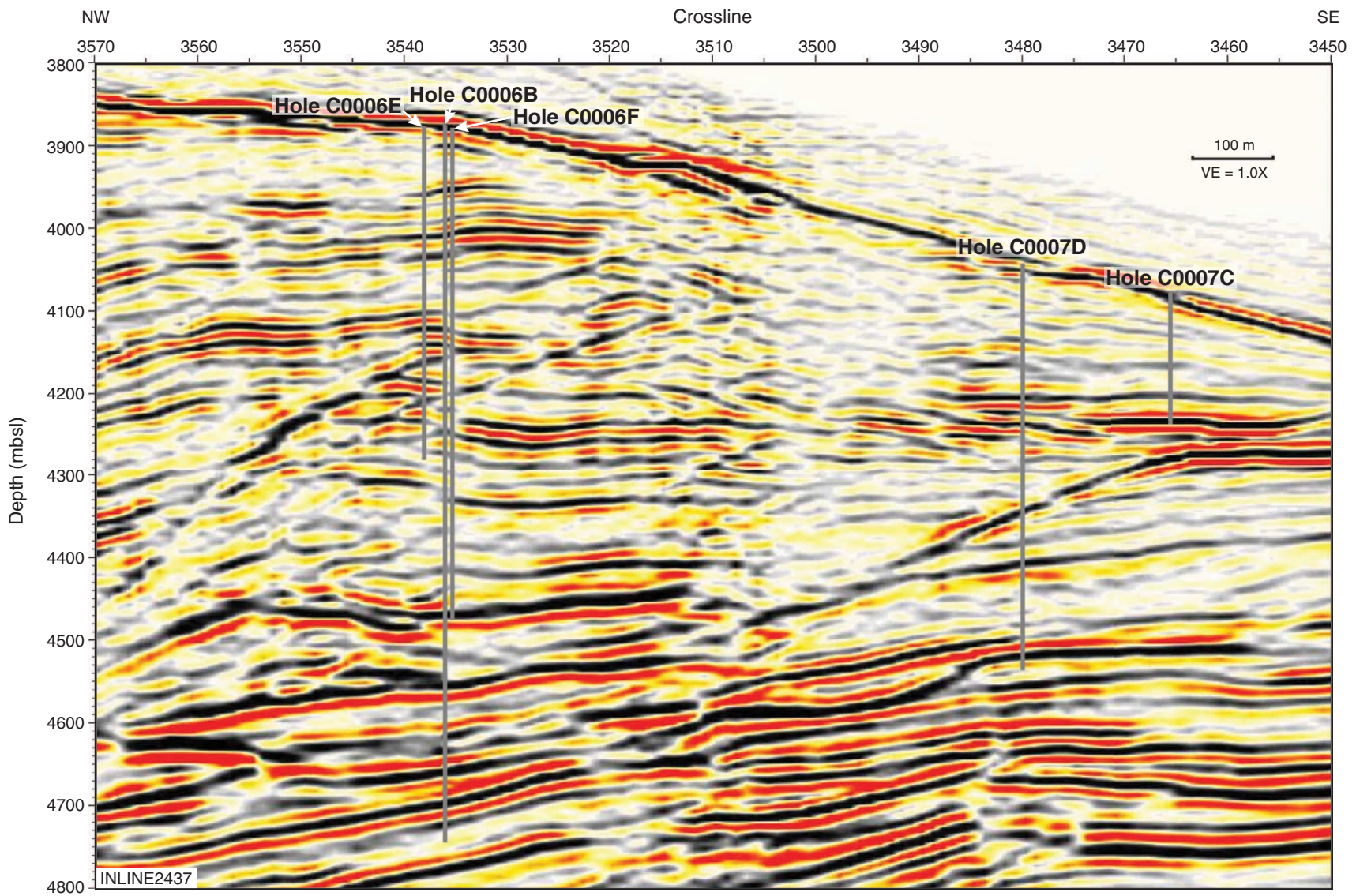
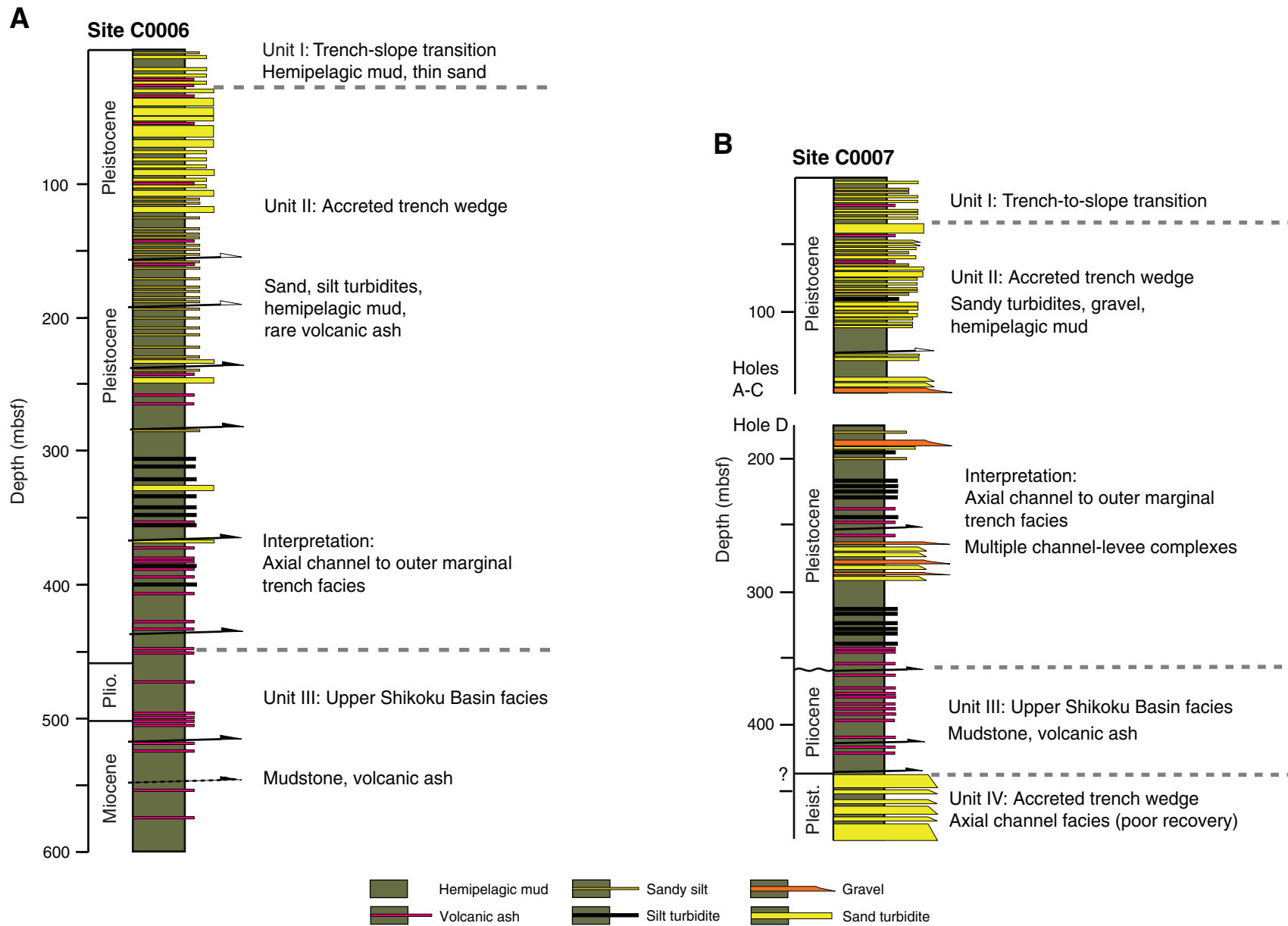


Figure F5. Three-dimensional seismic profile crossing Sites C0006 and C0007 (after Kimura et al., 2008). VE = vertical exaggeration.





**Figure F6.** Summary of lithostratigraphic units for (A) Site C0006 and (B) Site C0007. (Modified from M. Underwood's unpublished “official” stratigraphy columns for Expedition 316 drill sites; [jamstec-cdex.projectpath.com/P17230024/](http://jamstec-cdex.projectpath.com/P17230024/)).



**Figure F7.** Representative vector end point diagrams (Zijderveld, 1967) showing the results of (A) alternating-field and (B) thermal demagnetization for sedimentary rock samples from Expedition 316 drill sites with well-defined reversed and normal polarity ChRM magnetization. Samples 316-C0004C-1H-1, 37–37 cm, 316-C0007D-11R-1, 3–5 cm, and 316-C0004D-54R-1, 16–18 cm, are normally magnetized; Samples 316-C0008A-25H-1, 95–97 cm, 316-C0006E-20X-6, 27–29 cm, 316-C0008A-34X-1, 49–51 cm, and 316-C0006E-39X-7, 8–10 cm, are reversely magnetized. NRM = natural remanent magnetization. Straight lines in A indicate ChRM component using principal component analysis (Kirschvink, 1980). Black and open squares in B indicate projection of the magnetization vector end-point on the horizontal and vertical planes, respectively. (Continued on next page.)

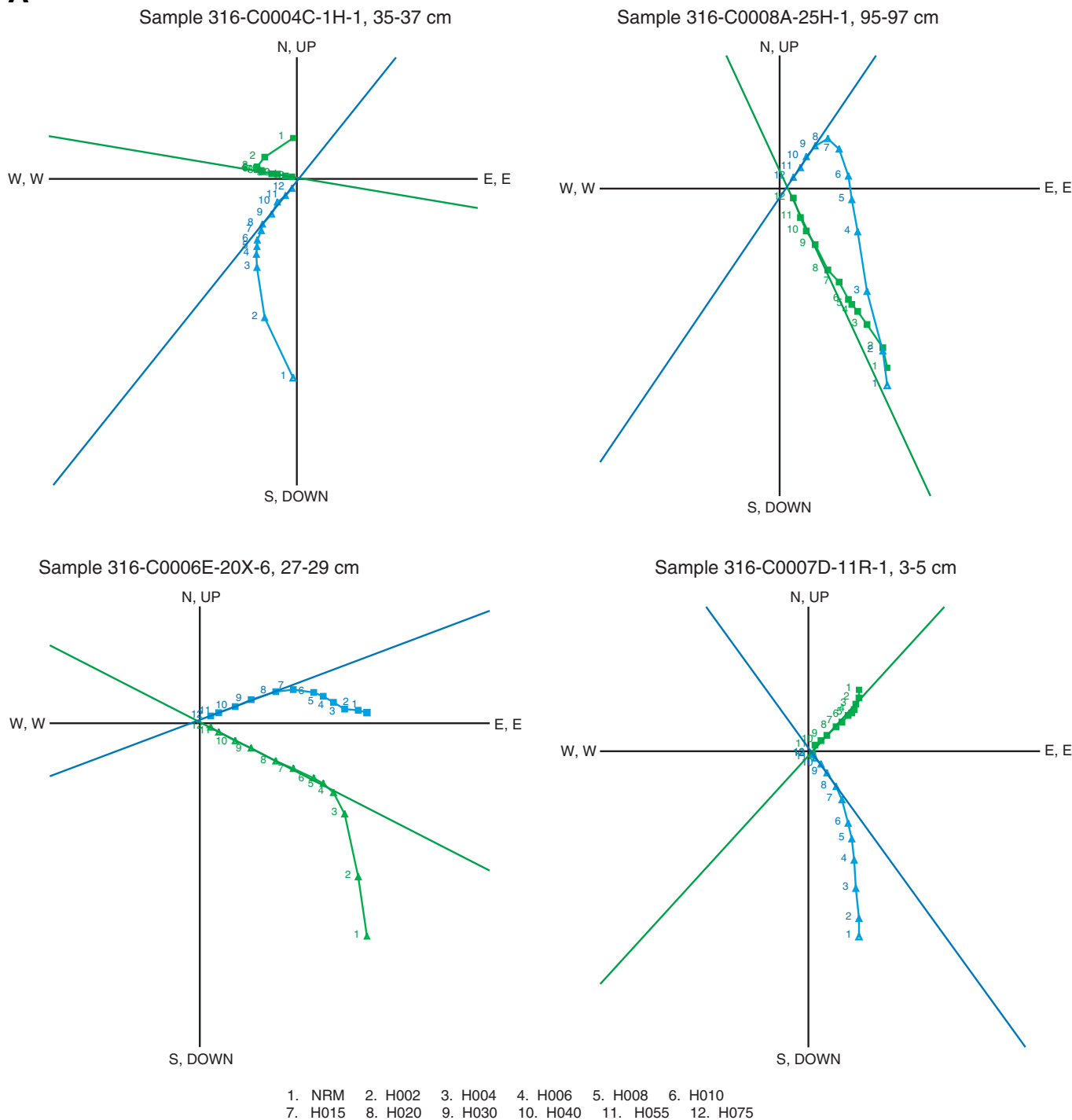
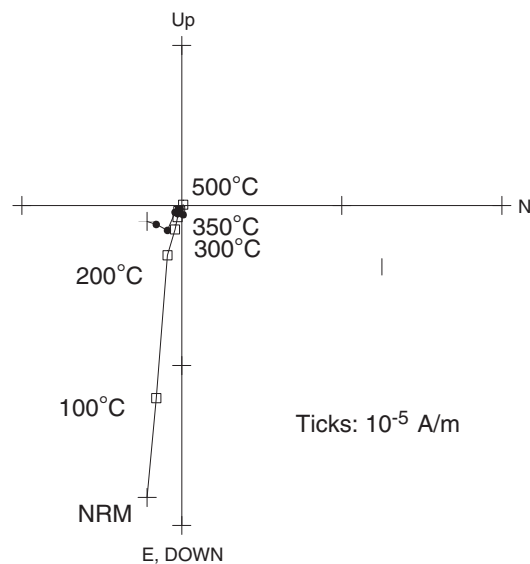
**A**

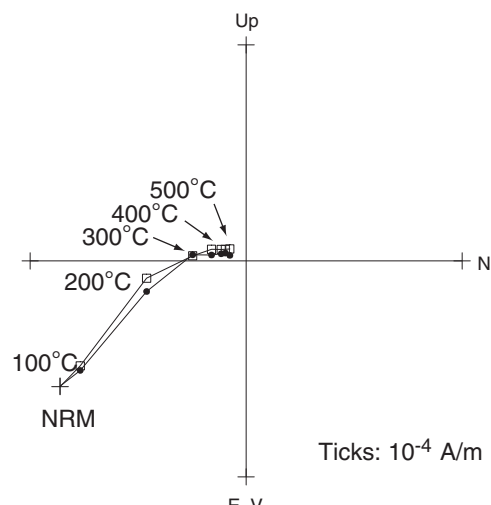
Figure F7 (continued).

**B**

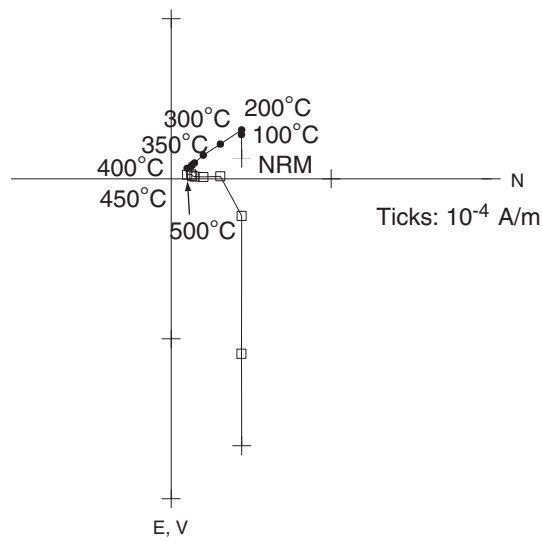
Sample 316-C0004D-54R-1, 16-18 cm



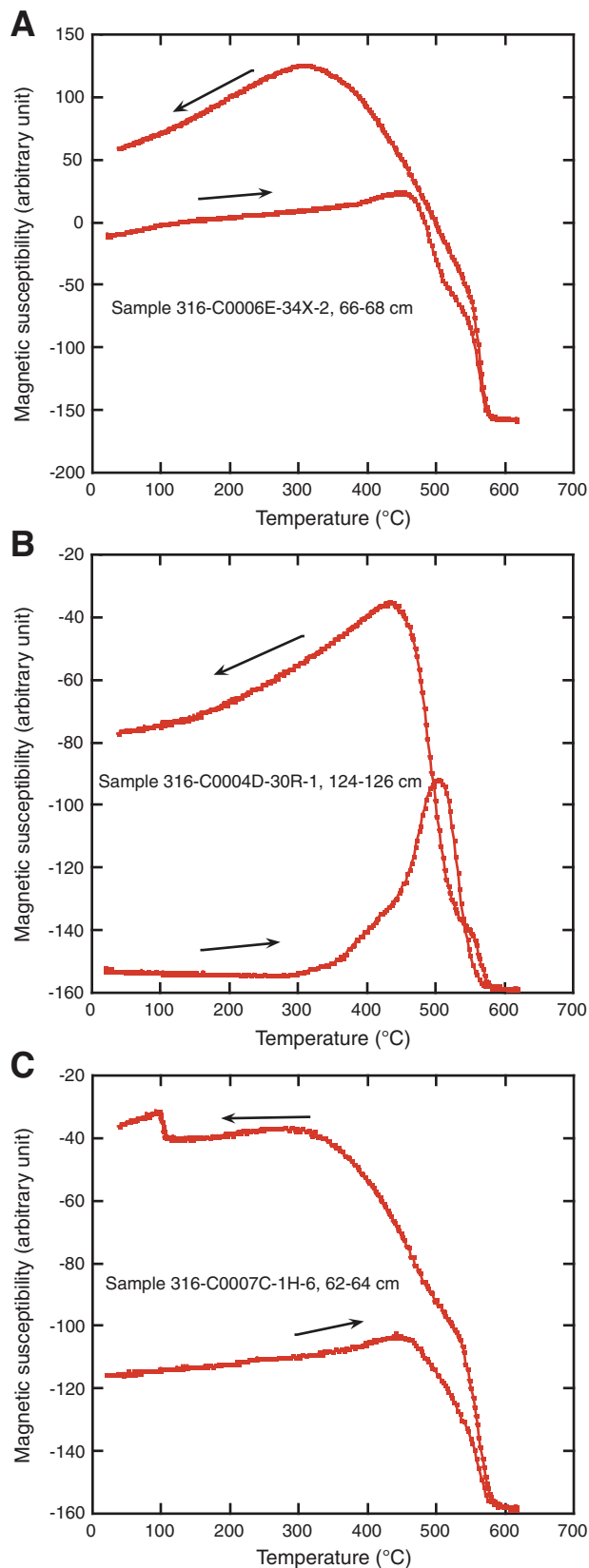
Sample 316-C0008A-34X-1, 49-51 cm



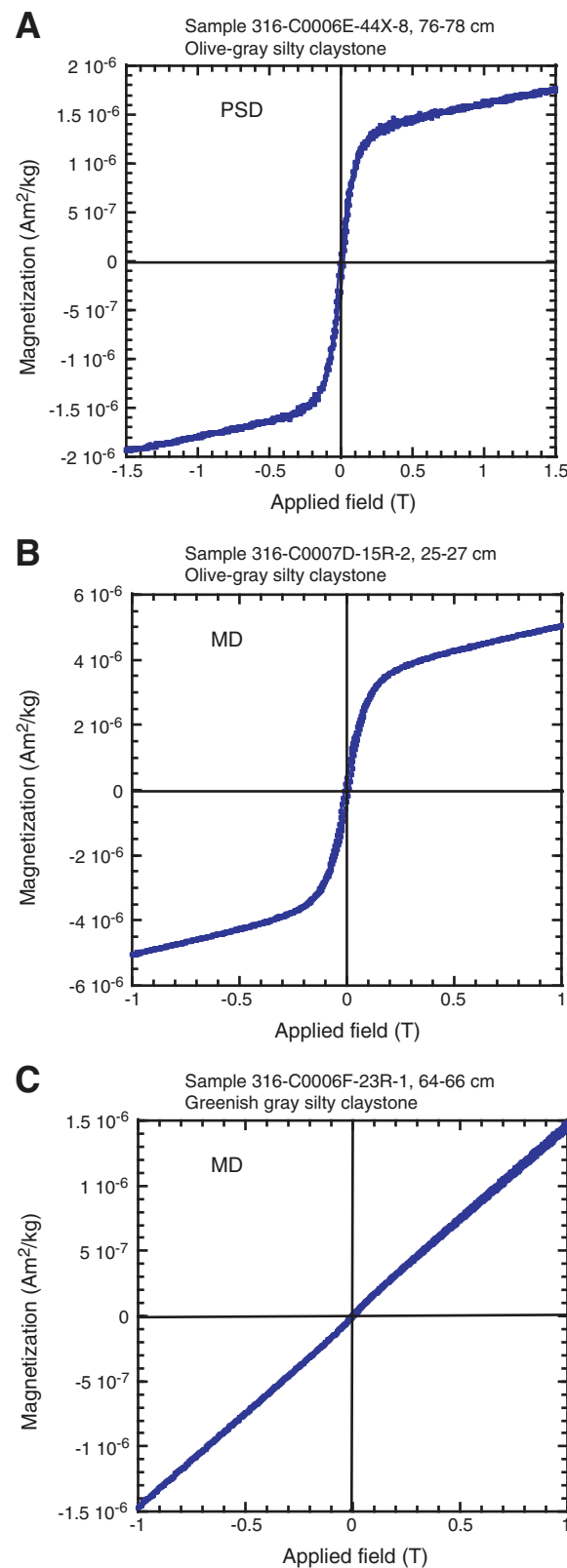
Sample 316-C0006E-39X-7, 8-10 cm



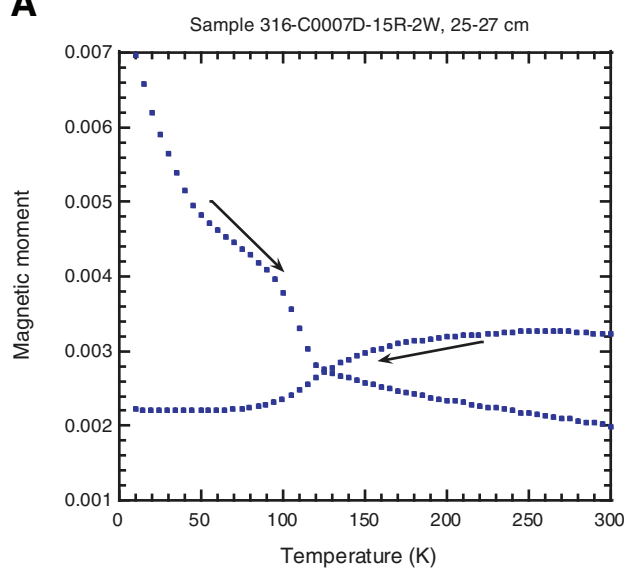
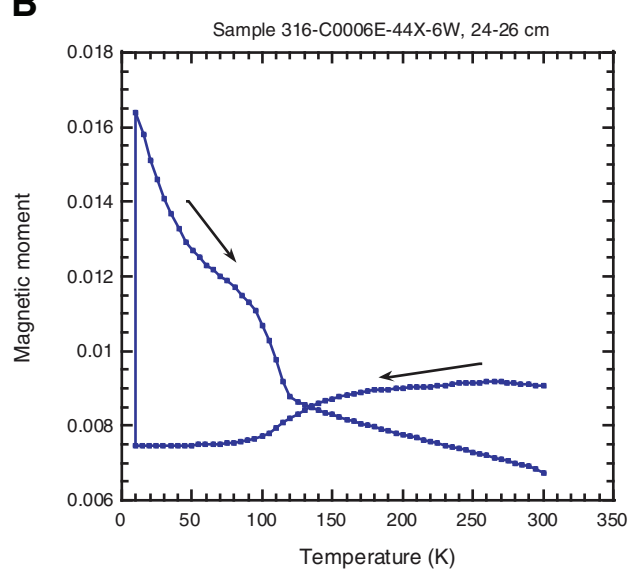
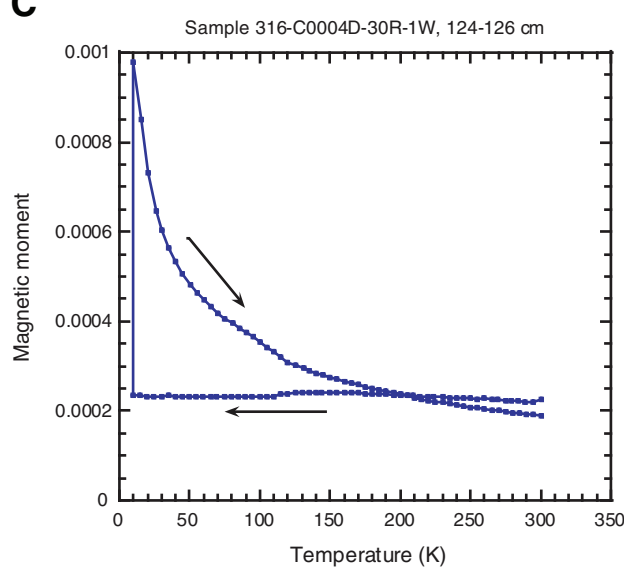
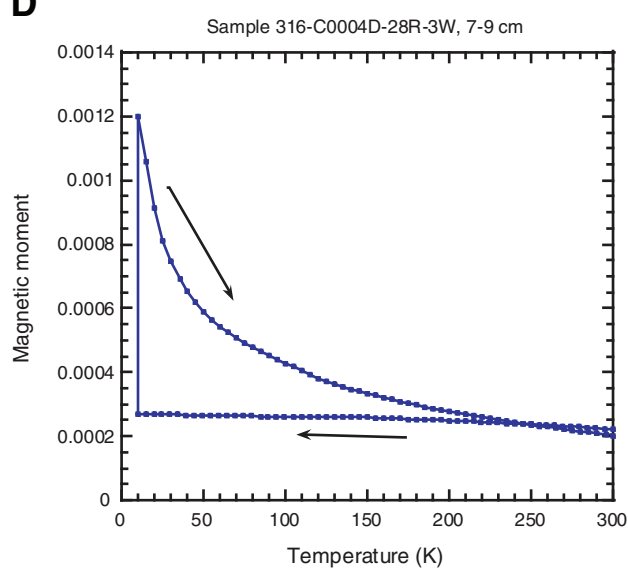
**Figure F8.** Typical thermomagnetic curves for representative samples. Directions of arrows indicate heating and cooling curves. A. Sample 316-C0006E-34X-2, 66–68 cm. B. Sample 316-C0004D-30R-1, 124–126 cm. C. Sample 316-C0007C-1H-6, 62–64 cm.



**Figure F9.** Diagrams of room-temperature hysteresis loops for representative rock samples in this study that exhibit pseudosingle domain (PSD) and multidomain (MD) behavior. Horizontal axis is applied field up to 1 T. Vertical axis is normalized magnetization (not corrected for slope). A. PSD Sample 316-C0006E-44X-8, 76–78 cm. B. MD Sample 316-C0007D-15R-2, 25–27 cm. C. MD Sample 316-C0006F-23R-1, 64–66 cm.



**Figure F10.** Low-temperature variations of saturation isothermal remanence for several representative samples during zero-field cooling from 300 to 10 K and zero-field warming back to 300 K that display behavior of different groups of low-temperature magnetometry (see text). Directions of arrows indicate heating and cooling curves. **A.** Sample 316-C0007D-15R-2W, 25–27 cm. **B.** Sample 316-C0006E-44X-6W, 24–26 cm. **C.** Sample 316-C0004D-30R-1W, 124–126 cm. **D.** Sample 316-C0004D-28R-3W, 7–9 cm.

**A****B****C****D**

**Table T1.** Summary of paleomagnetic data of sediments and rocks from Expedition 316. (Continued on next eight pages.)

Core, section, interval (cm)	Depth (mbsf)*	Demagnetization type	Range (mT/°C)	Declination (°)	Inclination (°)	Polarity	NRM intensity (A/m)	MAD (°)
316-C0004C-								
1H-1, 35–37	0.350	AF	20–75	279.5	51	N	4.74E–02	4
1H-2, 46–48	1.775	AF	30–75	260.5	42.3	N	3.90E–02	2.5
1H-4, 45–47	3.285	AF	20–55	297.1	49.7	N	7.08E–03	7.1
1H-5, 41–43	4.65	AF	20–55	230.6	70.1	N	3.91E–03	10.7
1H-7, 4–6	5.69	AF	30–75	231.6	52	N	1.15E–02	15.3
2H-1, 72–74	7.1	AF	20–55	170.6	53.7	N	2.96E–03	10.3
2H-2, 63–65	8.417	AF	20–55	152.9	39.7	N	1.41E–03	19.2
2H-4, 18–20	9.377	AF	20–55	217	53.5	N	1.44E–03	8
2H-5, 78–80	11.413	AF	6–15	162.3	63.5	N	2.58E–03	4.3
2H-6, 106–108	13.145	AF	6–30	172.9	62.1	N	2.41E–03	8.2
2H-8, 50–52	13.99	AF	6–55	151.8	54.8	N	2.15E–03	13.1
2H-9, 129–131	16.194	AF	8–40	128.6	51.6	N	5.75E–04	9.8
3H-1, 71–73	16.59	AF	10–20	52.7	50.2	N	1.58E–03	10.3
3H-1, 112–114	17	AF	10–20	144.2	49.6	N	6.14E–04	14.9
3H-3, 19–21	18.668	AF	15–40	155.6	60.6	N	8.61E–04	11.3
3H-4, 14–16	18.833	AF	15–40	265.1	38	N	6.24E–04	9.1
3H-6, 83–85	20.948	AF	8–30	88.9	53.8	N	5.65E–04	10.6
3H-7, 42–44	21.973	AF	8–15	211.9	67.4	N	7.28E–04	2.9
3H-9, 32–34	23.298	AF	30–75	237.4	38.6	N	5.41E–04	8.8
4H-1, 15–17	25.53	AF	4–75	270	15.5	N	4.62E–03	2.9
4H-2, 48–50	27.275	AF	30–75	307	34.1	N	5.95E–03	6.4
4H-3, 42–44	28.635	AF	20–55	350.8	34.3	N	7.18E–03	8.9
4H-6, 39–41	31.445	AF	10–55	101.4	49.4	N	1.34E–03	4.7
4H-7, 71–73	33.205	AF	8–30	206.3	38	N	2.14E–03	9.1
4H-8, 45–47	34.365	AF	30–75	276.4	54.4	N	1.01E–03	10.3
5H-1, 33–35	35.21	AF	6–20	63.5	72.9	N	6.89E–04	9.6
5H-2, 122–124	37.535	AF	NRM–6	331.1	84.4	Unstable	1.34E–03	1.2
5H-3, 47–49	38.28	AF	8–15	292.7	64.8		1.21E–03	11.6
5H-5, 44–46	39.72	AF	10–20	21.7	60.1	N	8.10E–04	15.6
5H-6, 52–54	41.305	AF	15–30	68.3	36	N	7.19E–04	11
5H-7, 32–34	42.56	AF	20–55	119.8	–20.3	R	5.09E–04	7
6H-1, 35–37	44.73	AF	40–75	83	–3.2	R?	1.57E–03	9.4
6H-2, 37–39	46.175	AF	55–75	105.8	–4	R?	9.65E–04	NA
6H-3, 39–41	47.64	AF	55–75	95.6	–62.2	R?	9.31E–04	NA
6H-5, 52–54	49.21	AF	75	27	–30.6	R?	2.11E–03	NA
6H-6, 54–56	50.685	AF	55	25.5	–37.2	R?	1.25E–03	NA
6H-7, 80–82	52.405	AF	75	19.2	–21.9	R?	1.57E–03	NA
6H-8, 71–73	53.825	AF	55	353	–55.9	R?	1.18E–03	NA
7H-1, 123–125	55.11	AF	8–15	317.8	30.3	N	1.83E–03	8.7
7H-2, 30–32	55.597	AF	10–15	230.2	42.4	N	3.33E–03	NA
7H-3, 19–21	56.917	AF	55–75	66.1	–52.5	N	3.17E–03	12.8
7H-4, 9–11	58.014	AF	15–40	112.2	62.3	N	5.53E–03	4.1
7H-5, 30–32	58.439	AF	30–75	86.3	43.3	N	2.63E–03	16.2
7H-7, 41–43	59.966	AF	15–30	286.4	46.4	N	2.62E–03	12.3
7H-8, 13–15	61.096	AF	15–30	40.4	44.6	N	3.57E–03	16.4
7H-9, 113–115	63.51	AF	15–30	64.4	33.9	N	3.81E–03	3.7
8H-1, 14–16	63.52	AF	30–75	304.9	–27.3	R	4.10E–03	8.9
8H-2, 96–98	65.74	AF	10–30	52.3	64.6	N	2.57E–03	9.4
8H-3, 110–112	67.29	AF	15–75	286.8	13.3	N	3.46E–03	5
8H-5, 19–21	68.035	AF	30–55 m	322.8	–20.5	R	3.35E–03	13
8H-6, 51–53	69.585	AF	40–75	337	–35.4	R?	7.91E–04	20.1
8H-7, 67–69	71.17	AF	8–15	154.4	63.2	N	2.29E–03	2.8
8H-8, 68–70	72.59	AF	30–55	285.5	37.4	N	4.31E–03	2.8
9H-1, 84–86	73.72	AF	10–30	2.9	64.7	N	7.94E–03	11.4
9H-2, 85–87	75.142	AF	6–75	146.2	–38.4	R	2.02E–02	4.4
9H-3, 90–92	76.602	TD	500	131	–19.9	R	3.47E–01	NA
9H-5, 33–35	77.689	AF	90	265.5	20.3	N	3.17E–01	NA
9H-5, 50–52	77.859	AF	2–15	52.8	–15.9	R	1.78E–03	10.9
9H-5, 84–86	78.199	AF	70	206.9	34.4	N	1.05E–04	NA
9H-5, 105–107	78.409	AF	NRM–2	157.1	–49.8	R?	1.28E–04	NA
9H-6, 42–44	79.01	AF	6–10	55.8	62.2	N	1.06E–04	5.4
9H-7, 53–55	80.534	AF	NRM–4	218.6	–51.6	R?	8.44E–04	0.2
10H-1, 86–88	81.7	AF	8–20	293.2	36	N	1.27E–02	3
10H-2, 82–84	83.095	AF	30–75	81.3	–67.1	R	6.50E–03	11.5
10H-4, 41–43	84.1	AF	20–75	158.7	–37.2	R	6.17E–03	7.1
10H-4, 45–47	84.14	TD	400	344.3	–49.7	R	4.31E–01	NA

**Table T1 (continued).** (Continued on next page.)

Core, section, interval (cm)	Depth (mbsf)*	Demagnetization type	Range (mT/°C)	Declination (°)	Inclination (°)	Polarity	NRM intensity (A/m)	MAD (°)
11H-1, 55–57	85.35	AF	20–55	79.7	20.6	N	7.03E-03	10.7
11H-3, 69–71	87.15	AF	20–55	134.9	34.1	N	9.09E-03	4.8
11H-4, 70–72	88.356	AF	20–40	120.6	54.4	N	1.01E-02	3.2
12X-1, 80–82	90.02	AF	30–55	157	-64.6	R	1.23E-02	12
12X-2, 90–92	91.3	AF	40–75	317.8	-20	R	1.57E-02	16.5
12X-3, 104–106	92.845	AF	30–55	83	-48.9	R	5.72E-03	15.1
12X-4, 117–119	94.38	AF	20–55	219.8	47.5	N	8.91E-03	3.7
12X-7, 107–109	96.335	AF	8–15	85	61	N	7.18E-03	1.5
12X-8, 68–70	97.355	AF	8–20	15.9	32.4	N	6.01E-03	1.8
12X-9, 26–28	98.345	AF	40–75	73.6	-11.8	R?	1.49E-02	0.8
13X-1, 54–56	99.26	AF	15–55	101.5	66.7	N	8.50E-03	6.1
13X-2, 55–57	100.68	AF	6–15	16.9	43.1	N	9.14E-03	1.6
13X-4, 55–57	102.085	AF	4–75	154.9	39.1	N	1.41E-02	1.6
13X-5, 39–41	103.385	AF	20–75	184.8	66.4	N	7.95E-03	13
13X-7, 74–76	106.515	AF	6–20	114.6	55.9	N	7.86E-03	2.6
13X-8, 19–21	107.37	TD	500	179.85	-22	R	1.29E-02	NA
13X-8, 31–33	107.49	TD	500	171.6	20.5	N	7.83E-03	NA
13X-8, 36–38	107.52	AF	30–55	357.2	15.4	N	2.25E-03	11.7
14X-1, 114–116	109.36	AF	40–75	147.7	67.3	N	4.75E-03	8.8
14X-2, 77–79	110.415	AF	20–55	46.9	61.1	N	3.23E-03	6.9
14X-3, 94–96	111.97	AF	6–30	60.9	57.5	N	4.91E-03	4.4
14X-4, 16–18	112.595	AF	10–30	78.7	60.3	N	6.96E-03	2.8
14X-6, 120–122	115.06	AF	NRM-6	338.8	55.9	N	8.88E-03	4.5
14X-7, 87–89	116.135	AF	10–30	11.9	55.7	N	7.41E-03	3.4
14X-8, 49–51	117.16	AF	8–30	52.4	63.6	N	4.05E-03	1.1
15X-2, 35–37	119.48	AF	6–20	325.4	37.4	N	8.60E-04	9.4
15X-3, 16–18	120.7	AF	10–20	212.7	34.5	N	9.56E-04	10.1
15X-4, 42–44	122.37	AF	6–20	190.2	36.8	N	2.31E-03	4.7
15X-5, 32–34	123.675	AF	5–30	87.5	31.7	N	4.59E-04	13.6
15X-6, 35–37	125.115	AF	15–40	326.2	36	N	7.63E-04	2.6
15X-8, 69–71	126.875	AF	30–55	45.3	35.1	N	4.39E-04	13.8
16H-1, 110–112	128.32	AF	8–20	305.3	51.2	N	5.02E-04	5
16H-2, 14–16	128.565	AF	2–15	348.2	36.8	N	6.20E-04	5.5
17H-1, 29–31	132.97	AF	10–30	259.4	-10.6	R	1.35E-03	7.2
18H-1, 70–72	133.88	AF	15–75	206.4	-47.5	R	1.34E-02	1.7
<b>316-C0004D-</b>								
1R-1, 91–93	100.91	AF	20–75	333.3	-34.7	R	5.49E-03	16.1
1R-2, 81–83	102.22	AF	30–55	51.5	76.6	N?	1.25E-03	7.4
2R-1, 28–30	109.78	AF	10–55	328.4	-36.1	R	1.51E-03	6.3
3R-3, 19–21	120.29	AF	30–55	251.5	62	N	2.89E-03	6.2
4R-1, 33–35	128.83	AF	10–40	340.3	44.7	N	1.85E-03	11.1
5R-1, 72–74	138.22	AF	20–40	85.5	29.5	N	8.65E-04	9.9
5R-2, 9–11	138.91	AF	15–30	49.8	64.4	N	1.13E-03	7.7
5R-4, 25–27	140.11	AF	15–30	147.7	50.3	N	1.43E-03	8.8
7R-1, 24–26	151.74	AF	40–75	23.3	-65	R	2.44E-03	2.9
11R-1, 46–48	169.96	AF	15–40	196.8	45	N	7.60E-04	15
11R-2, 24–26	170.83	AF	15–55	72	32.5	N	2.13E-03	8.7
11R-3, 13–15	171.04	AF	40–75	141.2	45.7	N	1.58E-02	14.1
12R-1, 10–12	174.1	AF	10–20	218.7	29.5	N	1.10E-03	9.9
13R-1, 15–17	178.65	AF	15–40	243	44.3	N	1.76E-03	6.4
16R-1, 83–85	202.83	AF	30–75	262.9	63.3	N	6.99E-04	15.3
19R-1, 10–12	225.6	AF	40–75	280.8	73	N	4.35E-03	2.7
21R-1, 44–46	238.44	AF	20–55	87	40.4	N	6.12E-04	5.6
23R-1, 60–62	247.6	AF	10–20	37.7	38.8	N	3.33E-04	13
24R-2, 64–66	253.55	AF	30–75	211	38.2	N	4.30E-04	15.4
25R-1, 25–27	256.25	AF	40–75	297.3	-53.8	R	4.77E-04	9.8
25R-2, 0–2	257.41	AF	40–55	63.1	-31.4	R	1.91E-03	NA
27R-1, 16–18	265.16	AF	20–55	128.8	58.7	N	2.10E-03	10.1
27R-2, 11–13	266.52	AF	40–75	44.7	39	N	9.01E-04	16.1
28R-1, 80–82	270.3	AF	30–55	274.5	66.8	N	2.34E-03	6.3
28R-2, 15–17	271.06	AF	30–75	13.9	-8.6	R?	1.36E-03	16.5
28R-3, 45–47	272.77	AF	6–10	203.2	76.6	N	1.24E-03	9.6
29R-1, 31–33	274.31	AF	20–55	218	28.3	N	1.65E-03	8.8
29R-2, 69–71	276.09	AF	20–40	11	43.2	N	1.76E-03	5.5
30R-2, 12–14	280.03	AF	15–40	200.3	51.5	N	2.04E-03	4
30R-3, 26–28	281.58	AF	15–30	23.4	33	N	2.29E-03	10.8
31R-1, 39–41	283.39	AF	15–40	340.6	-7.6	R	7.95E-04	6.6
31R-2, 38–40	284.79	AF	30–75	54.7	50	N	1.21E-03	1.4
32R-1, 21–23	287.71	AF	15–40	23.5	-26	R	2.21E-02	3.7

**Table T1 (continued).** (Continued on next page.)

Core, section, interval (cm)	Depth (mbsf)*	Demagnetization type	Range (mT/°C)	Declination (°)	Inclination (°)	Polarity	NRM intensity (A/m)	MAD (°)
32R-3, 36–38	290.67	AF	20–55	279	55.1	N	2.20E-03	13.7
32R-4, 18–20	291.5	AF	20–55	89.5	46.4	N	2.51E-03	7.2
33R-1, 12–14	291.12	AF	6–10	279.4	67.1	N	3.36E-03	7.7
33R-2, 10–12	293.51	AF	10–30	246.5	66.7	N	9.95E-4	10
33R-3, 10–12	294.92	AF	30–75	299.4	38.4	N	1.00E-03	15
33R-3, 62–64	295.44	AF	30–75	169.6	22.7	N	8.23E-04	18.9
34R-2, 0–2	297.91	AF	15–40	352.5	72.5	N	9.06E-04	1.2
35R-1, 62–64	301.13	AF	15–55	231.6	48.4	N	1.26E-03	4
35R-2, 2–4	302.43	AF	20–55	6.4	4.2	N	3.63E-03	3.2
36R-1, 62–64	306.12	AF	10–30	30.6	72.9	N	2.21E-03	2.1
36R-3, 8–10	306.99	AF	15–30	183.9	62.8	N	6.07E-04	10.5
37R-1, 90–92	310.9	AF	20–40	38.1	68.4	N	4.92E-03	3.3
37R-2, 80–82	312.21	AF	15–75	89.3	44.7	N	1.41E-02	11.7
39R-1, 19–21	319.19	AF	20–40	48	-39.7	R	2.07E-03	2.6
39R-1, 44–46	319.44	AF	15–40	157.1	57.7	N	6.71E-03	6.2
39R-1, 65–67	319.65	AF	30–55	265.1	9.7	N	5.13E-02	11.9
39R-3, 73–75	321.14	AF	15–30	276.5	69.3	N	2.51E-02	9.3
40R-2, 21–23	325.11	AF	20–55	219.2	50.2	N	5.33E-03	16.8
41R-3, 45–47	330.07	AF	15–30	160.9	37	N	9.01E-03	1.4
42R-1, 35–37	332.85	AF	40–75	124.6	-31.3	R	2.13E-02	12.5
42R-2, 8–10	333.98	AF	40–75	76.9	-4.1	R	3.52E-03	5.1
42R-3, 62–64	335.53	AF	15–30	180.7	62.3	N	2.15E-03	6.8
42R-4, 10–12	335.79	AF	8–30	312	60.4	N	2.32E-03	18.9
42R-5, 40–42	336.35	AF	10–40	103.9	51.2	N	9.88E-03	4
43R-1, 35–37	337.35	AF	20–75	15.9	-38.7	R	1.76E-03	22.1
43R-3, 35–37	339.765	AF	8–15	357.4	47.6	N	1.78E-03	3.7
44R-1, 22–24	341.72	AF	10–30	47.5	40.4	N	3.29E-03	4.9
44R-2, 11–13	343.01	AF	30–80	268.8	-25.1	R	9.44E-03	7.1
44R-4, 53–55	344.84	AF	20–80	11.9	-13.1	R	3.94E-03	10.9
45R-1, 28–30	346.28	AF	10–40	154.1	65.1	N	2.80E-03	1
45R-1, 35–37	346.35	AF	15–30	50.2	33.9	N	1.85E-02	2.5
45R-2, 74–76	348.15	AF	15–30	193.3	69.6	N	5.26E-03	8.3
46R-1, 12–14	350.62	AF	30–55	103.9	12	N	1.89E-02	8.8
46R-2, 3–5	351.94	AF	30–55	356.4	-28.1	R	2.22E-03	5.7
47R-3, 11–13	357.93	AF	20–55	134.9	61.3	N	7.58E-02	7.5
52R-1, 49–51	377.99	AF	20–55	354.8	-7.2	R	1.63E-02	5.9
52R-2, 39–41	379.29	TH	200–500	46.2	-18.5	R	2.15E-01	NA
53R-1, 12–14	382.12	AF	20–75	177.1	-32	R	3.84E-02	7.2
53R-1, 59–61	382.59	TD	400	293.82	43.49	N	4.37E-01	NA
53R-2, 31–33	383.715	AF	30–75	198.8	1.6	R?	1.87E-02	7.5
54R-1, 16–18	386.66	TD	350	116.6	51.2	N	1.91E-01	2.1
54R-1, 88–90	387.38	AF	20–40	59.2	37	N	2.05E-02	7.8
54R-2, 39–41	388.29	TD	400	260.28	55.8	N	2.65E-02	NA
54R-3, 28–30	390.25	AF	30–140	205.7	-31.3	R	4.49E-03	18.8
55R-1, 98–100	391.98	AF	20–75	75.9	39.1	N	9.93E-03	13.3
55R-1, 103–15	392.03	TD	500	28	67	N	8.97E-02	NA
55R-3, 28–30	394.1	AF	10–55	273.8	62.1	N	3.51E-03	6
56R-1, 138–140	396.88	TD	500	289.2	63.7	N	3.99E-01	NA
316-C0006C-								
1H-1, 15–17	0.15	AF	20–75	292.7	21.6	N	3.93E-03	6.8
1H-1, 17–19	0.17	AF	15–75	329.9	28	N	4.39E-02	4.1
1H-3, 27–29	1.75	AF	10–55	310.6	52.4	N	4.39E-02	4.1
1H-4, 5–7	3.03	AF	15–55	291.7	65.5	N	1.09E-03	7.1
1H-5, 8–10	4.535	AF	30–55	240.9	29	N	3.67E-03	4.6
1H-7, 16–18	6.345	AF	20–55	306.5	42.4	N	3.04E-03	7.3
1H-8, 113–115	8.645	AF	10–30	290.3	50.8	N	1.59E-02	9.2
316-C0006E-								
1H-1, 3–5	0.03	AF	10–75	77.6	54.8	N	3.31E-02	1.6
1H-1, 50–52	0.5	AF	8–30	268.2	36.3	N	1.97E-03	4.8
1H-3, 10–12	1.53	AF	6–10	312.3	55.1	N	4.02E-03	4.7
1H-4, 45–47	3.28	AF	6–15	329.4	57.4	N	1.17E-02	1.9
1H-6, 45–47	4.91	AF	8–20	339.3	48.8	N	1.02E-02	14.6
2H-1, 116–118	6.35	AF	30–75	75.3	36.6	N	3.04E-02	15.1
2H-2, 77–79	7.363	AF	15–40	202.5	39.3	N	1.76E-03	12.6
2H-4, 58–60	8.6	AF	4–8	111.9	43.9	N	2.77E-03	11.2
2H-5, 55–57	9.995	AF	15–75	192.7	62.1	N	1.50E-02	7.5
2H-6, 60–62	11.475	AF	8–15	193.2	64.4	N	6.68E-03	12
2H-8, 55–57	12.875	AF	8–30	212.9	54.1	N	2.47E-03	18.2

**Table T1 (continued).** (Continued on next page.)

Core, section, interval (cm)	Depth (mbsf)*	Demagnetization type	Range (mT/°C)	Declination (°)	Inclination (°)	Polarity	NRM intensity (A/m)	MAD (°)
2H-9, 65–67	14.45	AF	75–100	251.4	61.3	N	4.47E-03	6.6
3H-1, 67–69	15.36	AF	8–15	232	57.8	N	3.77E-03	0.8
3H-2, 14–16	16.235	AF	8–20	219.1	42.8	N	5.69E-03	8.4
3H-8, 26–28	22.145	AF	10–40	124.8	45.5	N	3.55E-03	19.9
3H-9, 9–11	23.385	AF	6–40	170.5	42.2	N	3.93E-03	4.7
4H-1, 45–47	24.64	AF	8–20	332	60.3	N	8.19E-03	2.7
4H-2, 12–14	25.745	AF	10–75	324.1	37.7	N	1.25E-02	6.8
4H-3, 28–30	27.315	AF	30–75	285.5	47.5	N	9.17E-02	10.5
4H-4, 10–12	28.54	AF	30–55	324.2	70.9	N	2.46E-02	0.5
4H-6, 14–16	30.295	AF	20–55	272.8	65.2	N	2.92E-02	10.6
5H-4, 57–59	36.625	AF	20–40	208.3	18.6	N	3.89E-02	4.6
5H-4, 69–71	36.745	AF	30–90	224	40	N	1.53E-01	4
5H-4, 92–94	36.965	AF	20–60	177.6	32.5	N	7.86E-02	4.1
5H-4, 114–116	37.195	AF	20–40	178.7	-59.9	R	2.03E-01	11.9
5H-4, 130–132	37.355	AF	20–60	169.5	21.8	N	1.38E-01	3.9
5H-5, 29–31	37.79	AF	30–90	186.3	63.5	N	2.91E-01	6.9
7H-1, 34–36	39.03	AF	20–75	127.2	52.5	N	1.93E-01	8.6
7H-2, 59–61	40.685	AF	20–55	102.3	53.3	N	9.04E-02	11.6
7H-3, 27–29	41.775	AF	15–55	87	46.6	N	9.28E-02	5.4
7H-5, 81–83	43.965	AF	15–75	68.3	51.3	N	8.39E-02	3.3
7H-6, 35–37	44.92	AF	15–40	85	56.2	N	2.70E-02	4
7H-7, 22–24	46.2	AF	40–75	131.4	-77.9	R?	8.40E-02	25.1
7H-8, 83–85	48.22	AF	15–75	287.7	-85	R?	4.76E-02	1.4
8H-1, 79–81	48.98	AF	30–55	11.9	77.2	N?	1.88E-01	8.5
8H-2, 55–57	50.135	AF	20–55	313.3	78.9	N?	7.47E-02	7.1
8H-3, 58–60	51.59	AF	6–55	274.3	64.7	N	2.61E-01	3
8H-5, 47–49	52.5	AF	40–75	349.8	69.3	N	1.70E-01	13
8H-8, 115–117	57.43	AF	30–75	17.2	44	N	1.23E-01	14.3
9H-1, 88–90	58.57	AF	8–15	200.5	42.5	N	7.54E-02	3.5
9H-2, 9–11	59.195	AF	40–75	338.6	-57.8	R	4.18E-02	2.4
9H-3, 9–11	60.58	AF	30–55	15.1	-37.4	R	1.02E-01	8.4
9H-6, 49–51	63.13	AF	40–80	153.6	-69.5	R	5.13E-03	10.3
11H-1, 19–21	64.86	AF	20–55	21.6	52.9	N	1.19E-01	1.2
11H-5, 92–94	68.834	AF	40–75	207.8	-7.6	R	5.65E-02	4.2
12H-1, 14–16	71.62	AF	40–75	265	-21.5	R	1.36E-01	24.3
12H-2, 13–15	72.09	AF	20–75	201.1	48.8	N	1.34E-01	7.9
12H-3, 30–32	72.605	AF	4–8	81.3	43	N	1.04E-01	2.8
12H-4, 25–27	73.965	AF	30–75	310.6	31.7	N	9.38E-02	6.6
12H-5, 35–37	75.245	AF	8–15	346.1	42.2	N	1.41E-01	5.1
12H-7, 32–34	76.84	AF	8–15	359.7	52	N	2.11E-01	1.8
12H-8, 10–12	77.625	AF	8–15	247.2	54.3	N	8.37E-02	4
13H-1, 58–60	78.4	AF	30–55	94.9	44.4	N	2.03E-01	4.1
15X-1, 67–69	80	AF	40–60	258.5	13.9	N	3.00E-03	2.3
15X-3, 60–62	81.645	AF	30–90	70.8	7.3	N	6.49E-02	10.3
15X-5, 97–99	82.943	AF	30–60	298.6	-25.3	R	2.06E-01	15.2
15X-6, 129–131	84.308	AF	30–70	124.7	-14	R	3.85E-02	10
15X-6, 140–142	84.418	AF	30–80	349.3	30	N	1.16E-01	12.6
15X-7, 69–71	85.118	AF	30–70	75.4	52.4	N	1.96E-01	11.6
16X-1, 36–38	89.19	AF	30–75	156.9	-16	R	1.38E-02	6
16X-3, 30–32	90.64	AF	15–75	61.7	-41.9	R	1.08E-01	2.3
17X-1, 50–52	98.83	AF	30–75	327.8	2	N	6.01E-02	0.8
17X-4, 55–57	101.1	AF	30–55	358.2	42.2	N	6.11E-02	8.8
17X-5, 6–8	101.235	AF	20–75	142.4	-36.7	R	9.50E-02	1.8
18X-1, 29–31	106.62	AF	30–75	334.6	7	N	1.24E-01	13.9
19X-1, 13–15	115.96	AF	20–75	40	29	N	1.44E-01	5
19X-2, 15–17	117.07	AF	20–75	101.7	-13.7	R	7.66E-02	2.4
19X-3, 0–2	117.26	AF	30–75	262	-7.8	R	6.59E-02	1.5
19X-4, 4–6	118.705	AF	30–75	278.5	-8.3	R	8.75E-02	3.1
19X-6, 10–12	120.18	AF	55–75	27.1	56.8	N	2.82E-01	NA
20X-1, 23–25	125.56	AF	90	336.5	-40.3	R	2.03E-01	NA
20X-1, 78–80	136.11	AF	30–55	151	-2.1	R?	3.38E-01	6.6
20X-2, 45–47	127.195	AF	30–50	89.8	37.7	N	1.08E-01	2.4
20X-3, 58–60	128.74	AF	10–75	37.8	67.1	N	8.48E-02	2
20X-4, 43–45	130.02	AF	90	277.6	-60.8	R	1.73E-01	NA
20X-4, 69–71	130.28	AF	55	198.8	15.6	N	2.17E-01	NA
20X-4, 108–110	130.67	AF	4–75	5.3	-21.2	R	2.53E-02	13.1
20X-5, 60–62	131.605	AF	20–55	273.9	5.3	R?	1.77E-02	3.3
20X-6, 27–29	132.685	AF	20–75	117.1	-18.5	R	2.08E-01	1.2
21X-1, 79–81	135.62	AF	30–75	142.8	-23.6	R	2.36E-02	6.8

**Table T1 (continued).** (Continued on next page.)

Core, section, interval (cm)	Depth (mbsf)*	Demagnetization type	Range (mT/°C)	Declination (°)	Inclination (°)	Polarity	NRM intensity (A/m)	MAD (°)
21X-2, 58–60	136.86	AF	20–40	246.8	33.5	N	6.11E-02	2.6
21X-4, 72–74	138.415	AF	20–70	222	-14.4	R	3.30E-02	4.1
21X-5, 10–12	139.205	AF	30–80	137.1	-6.3	R	4.47E-02	4.8
22X-1, 47–49	144.8	AF	30–80	331.5	94	N	6.70E-02	7.6
22X-4, 12–14	147.295	AF	60–80	315.8	76.9	N?	2.04E-01	13
22X-6, 5–7	150.045	AF	30–60	359.8	7.3	N	1.24E-01	4.8
23X-1, 72–74	154.55	AF	40–80	113.3	37.7	N	2.57E-02	NA
23X-2, 6–8	155.295	TD	500	230.5	83.3	N?	1.48E-01	NA
23X-3, 74–76	157.385	AF	40–70	281.5	-8.2	R	1.35E-02	NA
23X-5, 56–58	158.633	TD	500	245.39	45.1	N	9.78E-02	NA
23X-6, 87–89	160.355	AF	40–70	66	-35.8	R	5.84E-02	18
23X-7, 63–65	161.525	TD	500	199.2	-15.2	R	9.77E-02	NA
24X-1, 41–43	163.74	AF	20–40	272.2	-46.9	R	1.16E-01	2.1
24X-1, 108–110	164.41	TD	500	213	61.6	N	2.65E-01	NA
25X-1, 106–108	173.89	AF	20–60	19.4	46.5	N	7.24E-02	9
25X-2, 41–43	174.645	TD	500	227.87	60.79	N	2.09E-01	NA
25X-3, 90–92	176.54	AF	30–60	358.2	19	N	2.40E-02	3.8
25X-5, 94–96	179.397	AF	40–60	149.2	-30.4	R	2.73E-02	NA
25X-8, 31–33	181.437	AF	30–60	43.6	71.2	N	1.36E-01	10.7
26X-1, 114–116	183.47	AF	30–60	160.3	40.8	N	8.44E-02	13.6
26X-3, 72–74	185.955	AF	60–82	234.3	-24.3	R	7.49E-02	2.8
26X-6, 47–49	188.525	AF	30–70	39.1	-6.3	R	6.52E-02	4.7
26X-7, 30–32	189.762	AF	15–55	84.2	23.4	N	3.27E-02	9.2
26X-8, 71–73	191.587	AF	30–70	269.9	11.1	N	4.55E-02	1.9
27X-1, 109–110	192.92	AF	20–70	149.7	-44.9	R	1.13E-02	8.4
27X-2, 116–118	194.4	AF	6–55	0.2	36.7	N	1.85E-02	6
27X-3, 10–12	194.755	AF	20–70	328.2	0.8	R?	5.42E-02	6
27X-4, 78–80	196.855	AF	30–70	38.7	-23.8	R	4.57E-02	6.9
27X-6, 15–17	198.015	AF	30–70	75.1	-21.2	R	2.34E-02	7
27X-7, 15–17	199.065	AF	30–50	214.2	-0.5	R	8.93E-03	7.5
27X-8, 15–17	200.465	AF	30–50	150.5	0	R?	1.75E-02	12.4
28X-1, 50–52	201.83	AF	30–50	148	-27.5	R	1.63E-02	11.8
28X-2, 24–26	202.98	AF	40–70	91.7	16.5	N	2.20E-02	11.8
28X-4, 0–2	204.165	AF	15–40	316.4	29.4	N	3.47E-02	10.2
29X-1, 44–46	211.27	AF	40–70	129.4	49.8	N	5.96E-02	18.4
29X-2, 48–50	212.74	AF	30–50	242.3	58.1	N	2.25E-01	4.8
29X-3, 36–38	214.03	AF	20–40	76.5	51.9	N	6.81E-02	10.3
29X-4, 56–58	215.64	AF	30–50	165.8	-3.4	R	1.94E-02	17.4
29X-5, 23–25	216.72	AF	50–70	99.2	31.3	N	4.78E-02	12.7
29X-6, 3–5	217.98	TD	400	210.9	23.39	N	3.27E-02	NA
29X-6, 6–8	218.01	TD	400	283.66	29.36	N	3.68E-02	NA
29X-6, 11–13	218.06	TD	400	26.39	-7.5	R	3.58E-02	NA
29X-6, 25–27	218.4	TD	400	75.51	-3.96	R	4.74E-02	NA
29X-6, 30–32	218.25	TD	400	295.04	-12.6	R	5.73E-02	NA
30X-1, 51–53	220.84	AF	20–60	118.9	65.5	N	6.37E-02	6.9
30X-2, 41–43	222.15	AF	120	164.76	-45.1	R	1.69E-02	NA
30X-4, 15–17	223.685	AF	30–50	31.5	-29.6	R	1.56E-02	8.3
30X-6, 30–32	226.285	AF	40–70	331.4	7.7	N	5.97E-02	4.6
30X8, 67–69	229.394	AF	30–50	256.3	65.3	N	9.37E-02	10.9
31X-1, 91–93	230.74	AF	40–70	99.6	69	N	4.07E-01	5
31X-4, 17–19	232.855	AF	30–70	213.3	-9.3	R	1.10E-01	7.8
31X-5, 122–124	235.325	AF	30–70	113.3	58.7	N	3.20E-01	6.2
32X-1, 22–24	239.55	AF	40–70	66.2	-29	R	3.67E-02	2
32X-2, 42–44	241.175	AF	40–70	85.9	-12	R	4.22E-02	2.6
32X-3, 35–37	242.515	AF	30–50	153.6	-26	R	2.43E-02	3.3
32X-5, 67–69	244.26	AF	30–70	357.6	58	N	7.06E-02	1.9
32X-6, 39–41	245.395	AF	30–70	43.2	13.3	N	9.78E-02	9.9
32X-7, 4–6	246.455	AF	30–50	13.5	49.4	N	3.25E-01	13.8
32X-8, 12–14	247.445	AF	40–60	123.9	-45.9	R	1.98E-01	11.2
34X-1, 43–45	258.76	AF	30–75	316.5	-15.7	R	5.28E-02	3.8
34X-2, 66–68	260.4	AF	10–30	40	68.1	N	1.24E-01	3.6
34X-3, 50–52	261.65	AF	20–55	36.2	12.3	N	4.31E-01	3
34X-4, 64–66	263.21	AF	20–40	320.2	32.8	N	3.87E-02	7.3
34X-6, 96–98	264.955	AF	20–55	2328	-33.6	R	2.18E-02	9.2
35X-1, 12–14	267.95	AF	40–60	27.6	48.1	N	7.81E-02	15.6
35X-3, 45–47	269.505	AF	30–55	326.5	39.5	N	5.49E-02	8.9
35X-4, 55–57	271.01	AF	20–40	69	35.1	N	3.82E-02	3.7
36X-1, 51–53	277.84	AF	15–40	47.8	50.4	N	1.88E-01	2.1
36X-5, 89–91	282.81	AF	20–55	262	-2.2	R	1.46E-01	4

**Table T1 (continued).** (Continued on next page.)

Core, section, interval (cm)	Depth (mbsf)*	Demagnetization type	Range (mT/°C)	Declination (°)	Inclination (°)	Polarity	NRM intensity (A/m)	MAD (°)
37X-1, 38–40	287.21	AF	15–55	98.1	37.9	N	1.49E-01	2.7
37X-3, 120–122	290.85	AF	20–55	343.2	-31.6	R	1.12E-02	11
37X-4, 64–66	291.705	AF	15–30	45.8	38.8	N	5.59E-02	2.5
37X-7, 102–104	294.915	AF	20–55	33.1	-12.8	R	5.86E-02	5.4
39X-5, 24–26	310.305	AF	20–75	56.5	-1.2	R	9.78E-02	4.2
39X-5, 63–65	310.695	TD	500	309.7	-9.6	R	1.63E-01	NA
39X-5, 75–77	310.815	AF	80	301.8	-35.4	R	1.77E-01	NA
39X-7, 8–10	312.965	TD	500	326.5	-12.2	R	1.73E-01	NA
39X-7, 31–33	313.195	AF	20–75	340.2	-21	R	5.67E-02	2.9
39X-8, 36–38	314.655	AF	30–75	190	-19.2	R	7.13E-02	2.1
40X-4, 40–42	319.965	AF	15–40	308.1	35.5	N	8.81E-02	4
40X-6, 22–24	321.21	AF	15–40	198.4	3.8	N	4.28E-02	6
40X-8, 73–75	323.14	AF	80	278	-46.5	R	1.80E-01	NA
40X-8, 80–82	323.21	AF	80	47.7	4.2	R?	1.21E-01	NA
41X-1, 90–92	325.73	AF	15–40	359.3	45.8	N	1.61E-01	1
41X-2, 52–54	326.765	AF	20–75	20.8	32.5	N	3.92E-01	8.8
41X-5, 55–57	329.76	AF	30–55	230.9	-5.7	R	1.38E-01	6.9
43X-7, 104–106	351.945	AF	20–55	18.1	-22.2	R	2.22E-02	4
44X-3, 71–73	356.875	AF	40–75	95.6	-59.2	R	4.27E-02	11
45X-1, 91–93	363.74	AF	20–55	68.1	42	N	1.40E-01	6.3
45X-2, 3–5	364.255	AF	20–40	26.4	57.9	N	3.73E-02	6.3
45X-5, 3–5	367.08	AF	30–55	9.4	21.3	N	4.29E-02	9.6
45X-6, 98–100	369.445	AF	20–75	73	41.7	N	3.09E-01	6.1
45X-7, 5–7	369.925	AF	30–75	326.9	43	N	2.38E-01	5.3
46X-1, 48–50	372.81	AF	30–75	354.6	31.2	N	2.60E-02	2.4
46X-2, 37–39	374.12	AF	30–75	293.8	-0.5	R?	5.57e-2	8.9
47X-1, 84–86	382.67	AF	20–75	154.7	-0.2	R?	1.27E-01	9.8
47X-7, 5–7	387.545	AF	30–75	139.5	49.1	N	2.78E-01	0.9
48X-2, 61–63	393.35	AF	30–75	44.5	59.6	N	3.03E-01	1.6
316-C0007D-								
3R-1, 89–91	190.89	AF	10–40	117.9	46.6	N	9.45E-03	4.5
5R-2, 84–86	211.245	TD	350	326.9	-7.1	R	1.31E-03	NA
5R-cc, 5–7	211.335	TD	500	140.47	-30.83	R	1.09E-01	NA
6R-1, 93–95	219.43	TD	550	272.61	-11.33	R	7.26E-02	NA
6R-3, 41–43	220.865	TD	550	105.8	-10.83	R	2.90E-01	NA
8R-1, 49–51	257.99	TD	550	336.12	48.32	N	3.75E-01	NA
8R-2, 28–30	239.19	AF	20–40	273.5	55.1	N	2.18E-01	8
10R-1, 1–3	256.51	AF	30–55	348.6	65.6	N	1.65E-01	3.8
11R-1, 3–5	266.03	AF	15–55	49	49.5	N	1.27E-01	3.4
22R-1, 31–33	370.31	TD	600	105.4	50.4	N	9.24E-02	NA
22R-3, 21–23	373/03	TD	600	84.7	52	N	8.16E-02	NA
24R-2, 126–128	391.67	AF	30–55	1.7	-1.9	R	1.57E-03	15
24R-3, 29–31	392.13	TD	550	8.85	-7.14	R	3.86E-03	NA
24R-4, 6–8	393.31	AF	30–55	80.6	74.9	N	5.72E-01	6.7
25R-3, 48–50	401.845	AF	30–75	125.1	46.1	N	3.95E-03	12.2
25R-5, 23–25	404.42	AF	30–75	231.4	61.5	N	6.96E-01	19.1
316-C0008A-								
1H-1, 9–11	0.09	AF	20–75	11.2	44.6	N	3.09E-02	1.8
1H-2, 3–5	1.435	AF	30–75	329.6	57.3	N	2.59E-03	8.6
1H-2, 67–69	2.075	AF	10–15	47.6	65.9	N	1.51E-03	NA
1H-4, 9–11	1.945	AF	6–10	31.6	40.7	N	1.36E-03	1.6
1H-4, 11–13	1.965	AF	30–75	257.5	-20.6	R	2.21E-03	15.7
1H-5, 9–11	2.925	AF	8–20	316.6	62.7	N	4.32E-03	5
1H-5, 13–15	2.965	AF	30–75	133.3	-34.8	R	6.40E-03	13.7
1H-5, 56–58	3.395	AF	30–75	346.3	-1.9	R	1.05E-02	6.5
1H-6, 9–11	4.33	AF	20–40	285.8	58.7	N	1.56E-03	10.1
1H-7, 29–31	5.72	AF	20–55	329.8	42.1	N	1.45E-03	5.6
2H-1, 12–14	7.05	AF	8–15	13	13.6	N	8.40E-04	12.5
2H-3, 10–12	8.675	AF	30–75	194.4	50.2	N	2.05E-02	4.8
2H-4, 10–12	9.88	AF	8–30	258.6	76.7	N?	4.40E-03	10.4
2H-5, 10–12	11.315	AF	20–75	154.1	57.7	N	1.95E-02	8.8
2H-6, 10–12	12.745	AF	20–55	199	38.6	N	7.35E-03	3.7
2H-7, 30–32	14.375	AF	10–55	196	36.3	N	3.54E-03	4.4
2H-9, 10–12	15.76	AF	15–55	138.4	33.7	N	2.13E-03	11.8
3H-1, 72–74	16.22	AF	15–40	143.9	38.3	N	8.32E-04	15.2
3H-2, 72–74	17.655	AF	20–40	58.2	64.4	N	4.32E-03	5.8
3H-4, 68–70	19.32	AF	10–55	335.5	55.1	N	9.81E-04	7.9
3H-5, 74–76	20.66	AF	30–40	266.1	22.6	N	1.51E-03	NA

**Table T1 (continued).** (Continued on next page.)

Core, section, interval (cm)	Depth (mbsf)*	Demagnetization type	Range (mT/°C)	Declination (°)	Inclination (°)	Polarity	NRM intensity (A/m)	MAD (°)
3H-6, 41–43	21.795	AF	10–20	105.5	54.2	N	1.52E-03	12.8
3H-9, 29–31	23.505	AF	30–40	276	66.3	N	1.52E-03	NA
3H-10, 34–36	24.755	AF	15–40	300.1	62.9	N	1.55E-03	14.5
4H-1, 49–51	25.49	AF	30–55	193.4	31	N	2.32E-03	8.8
4H-2, 12–14	26.455	AF	30–75	174.8	-61.8	R	7.19E-03	14.6
4H-3, 29–31	27.935	AF	40–75	24.6	45.7	N	3.94E-03	18.5
4H-5, 81–83	30.22	AF	10–20	339.2	49.9	N	3.23E-03	8.9
4H-6, 107–109	31.63	AF	20–40	301.9	37.6	N	5.61E-03	5.1
4H-7, 103–105	32.97	AF	15–40	335.1	-15.3	R	3.01E-03	11.2
4H-8, 120–124	34.49	AF	8–15	307.8	46.4	N	2.06E-03	4
4H-9, 4–6	34.64	AF	10–20	14.5	20.2	N	9.04E-04	11.3
5H-1, 19–21	34.69	AF	30–55	321.1	-50.1	R	6.35E-04	20.7
5H-2, 15–17	35.975	AF	15–40	253.5	5.4	R?	4.62E-04	14.7
5H-3, 16–18	37.39	AF	40–75	1.6	-38.3	R	1.04E-03	12.5
5H-5, 40–42	39.335	AF	40–75	261.9	-43.6	R	8.59E-04	4.6
5H-6, 113–115	41.165	AF	55–75	30.4	-46.1	R	8.92E-04	NA
5H-7, 8–10	41.45	AF	15–40	66.2	41.6	N	4.52E-03	1.8
5H-8, 37–39	43.055	AF	15–30	112	-13	R	1.48E-03	17.2
5H-9, 32–34	44.315	AF	40–75	287.4	-26.8	R	5.19E-04	4.2
6H-1, 40–42	44.4	AF	30–55	250.1	65.8	N	8.43E-03	6.8
6H-2, 40–42	45.73	AF	40–100	130.2	60.2	N	4.61E-02	14.3
6H-3, 40–42	47.16	AF	20–55	25.6	57.2	N	1.53E-02	17.8
6H-6, 40–42	49.895	AF	20–40	6.6	-41.2	R	3.80E-03	10.1
6H-7, 40–42	51.225	AF	10–55	227.2	-29.3	R	4.86E-03	4
6H-8, 40–42	52.53	AF	8–30	129.4	-1.9	R	3.96E-03	1.8
6H-9, 40–42	53.835	AF	30–75	336.6	-40.8	R	4.20E-03	3.7
7H-1, 65–67	54.15	AF	30–75	14.9	-37.1	R	5.15E-03	15
7H-2, 65–67	55.465	AF	15–40	200.4	28	N	6.26E-03	5.1
7H-3, 65–67	56.825	AF	20–75	18.3	-13.7	R	4.89E-03	12.9
7H-4, 65–67	58.13	AF	30–75	329.4	-61.3	R	2.19E-03	6.2
7H-6, 60–62	59.44	AF	15–40	299	57.6	N	4.49E-03	10.2
7H-7, 65–67	60.92	AF	40–75	327.2	-52.9	R	1.57E-03	1
7H-8, 35–37	61.985	AF	40–55	151.7	-41.6	R	3.67E-03	NA
7H-9, 20–22	63.11	AF	20–55	29.5	-40.5	R	4.58E-03	6
8H-1, 20–22	63.21	AF	30–55	164	-47.7	R	5.51E-03	5.2
8H-2, 10–12	64.43	AF	20–55	225.1	-48.4	R	2.98E-03	5.9
8H-3, 10–12	65.73	AF	15–30	340.6	-53.1	R	1.36E-02	3.1
8H-4, 55–57	67.49	AF	30–55	157.8	-48.1	R	9.15E-04	5.9
8H-6, 10–12	68.58	AF	30–75	168.8	-26	R	1.45E-03	13.7
8H-7, 10–12	69.67	AF	55–75	254	-35.1	R	1.99E-03	NA
8H-8, 10–12	70.97	AF	40–75	244.8	-34.7	R	9.27E-04	24.2
9H-1, 10–12	72.6	AF	30–55	211.1	-4.1	R	1.40E-03	14.7
9H-2, 10–12	73.905	AF	20–55	246.3	-11.2	R	2.68E-03	8.4
9H-3, 10–12	75.22	AF	20–55	241.9	-11.5	R	1.62E-03	2.6
9H-4, 12–14	76.57	AF	30–55	262.2	-36.3	R	5.52E-03	15.2
9H-6, 1–3	77.84	AF	30–75	265.6	-29.5	R	2.55E-03	6.9
10H-1, 16–18	82.16	AF	10–30	74.6	57.3	N	4.42E-03	5.2
10H-2, 65–67	83.185	AF	20–40	359.5	-45.3	R	1.39E-03	6.8
10H-3, 41–43	83.925	AF	15–55	307.6	-46.8	R	4.22E-03	8.6
10H-4, 75–77	85.415	AF	30–55	354.1	-34.5	R	8.45E-03	10.6
10H-5, 33–35	86.415	AF	30–75	297.4	-43.5	R	2.61E-03	10.2
10H-7, 17–19	87.68	AF	15–40	328	-38.7	R	1.32E-03	7.3
10H-8, 55–57	89.47	AF	15–30	222.2	-14.6	R	1.48E-03	3.1
11H-1, 11–13	90.61	AF	30–75	305.3	-49.7	R	1.20E-03	7.3
11H-2, 19–21	92.21	AF	20–40	41.5	-17.1	R	8.14E-04	20.1
11H-3, 9–11	93.515	AF	20–75	93	-43.8	R	1.47E-03	17.6
11H-5, 13–15	95.14	AF	30–55	9.9	-65.2	R	2.24E-03	9.7
11H-6, 11–13	96.295	AF	15–55	7.6	-40.4	R	6.26E-04	7.1
11H-7, 17–19	97.87	AF	10–40	126.7	-21.8	R	6.14E-03	13.9
11H-8, 13–15	99.24	AF	20–40	24.8	-44.8	R	9.23E-04	6.1
12H-1, 53–55	100.53	AF	30–75	334	-42.9	R	2.30E-03	9.9
12H2, 16–18	101.065	AF	30–55	350.4	-27.8	R	2.77E-03	7.3
12H-3, 9–11	102.4	AF	20–75	29.1	-28	R	3.97E-03	4.1
12H-4, 15–17	103.87	AF	20–55	53.2	-37.6	R	1.26E-03	5.5
12H-6, 41–43	105.6	AF	30–55	8.6	-49.7	R	6.95E-04	9.5
13H-1, 46–48	109.96	AF	30–40	239	-12.8	R	1.09E-03	4.1
13H-2, 71–73	111.625	AF	40–75	61.9	-47.9	R	2.62E-03	11.4
13H-3, 36–38	112.685	AF	15–30	47.8	31.9	N	5.08E-03	6.8
13H-4, 36–38	114.1	AF	20–40	334.3	-62.2	R	7.69E-04	18.4

**Table T1 (continued).** (Continued on next page.)

Core, section, interval (cm)	Depth (mbsf)*	Demagnetization type	Range (mT/°C)	Declination (°)	Inclination (°)	Polarity	NRM intensity (A/m)	MAD (°)
13H-6, 6–8	115.135	AF	30–55	303	-12	R	4.27E-03	4.8
15H-3, 19–21	120.665	AF	40–75	196.1	53.7	N	2.80E-03	2.5
15H-6, 44–46	124.56	AF	20–55	356.5	59.5	N	9.33E-03	7.7
16H-1, 33–35	127.8	AF	15–30	358.7	72.3	N	4.45E-03	11.3
16H-3, 12–14	128.64	AF	10–30	300.7	-12	R	6.87E-03	5.8
16H-5, 39–41	129.49	AF	20–75	256	-60	R	2.31E-03	8.6
17H-2, 10–12	131.255	AF	40–75	20.4	-17.7	R	5.37E-03	4.3
17H-4, 66–68	134.435	AF	20–40	171.6	4.2	N	1.20E-03	NA
17H-5, 40–42	135.495	AF	10–20	10.4	43.7	N	3.12E-03	19.1
18H-1, 55–57	140.94	AF	40–75	308	-61.7	R	8.02E-04	12.8
18H-2, 65–67	142.36	AF	30–55	243.1	63.5	N	2.93E-03	1.7
18H-4, 55–57	143.835	AF	10–75	338.9	-59.2	R	1.51E-03	5.8
18H-5, 55–57	144.88	AF	20–40	264.9	42.7	N	2.77E-03	3.6
18H-6, 55–57	146.025	AF	10–30	340.1	33.5	N	1.95E-03	8.3
18H-7, 55–57	146.875	AF	8–15	147.8	54.3	N	5.15E-04	13.5
18H-8, 65–67	147.93	AF	8–15	39.7	49.4	N	2.41E-03	6
19H-1, 46–48	150.35	AF	20–40	195.3	26.9	N	2.49E-03	8.8
19H-3, 9–11	151.74	AF	40–75	163.2	-55	R	2.13E-03	14.9
21H-1, 110–112	159.83	AF	80	48.97	-26.1	R	3.83E-02	NA
21H-2, 110–112	161.235	AF	80	40.26	-48.57	R	3.07E-02	NA
21H-6, 25–27	164.655	AF	80	23.81	-30.24	R	4.74E-02	NA
22H-2, 62–64	169.12	AF	80	347.75	-35.32	R	3.67E-02	NA
23H-2, 58–60	179.615	AF	80	40.47	-34.88	R	5.92E-02	NA
24H-2, 97–99	188.655	AF	100	133.25	-64.38	R	7.03E-02	NA
24H-4, 127–129	191.575	AF	100	254.85	-44.71	R	3.46E-02	NA
25H-1, 60–62	197.33	AF	80	340.58	-45.62	R	6.62E-02	NA
25H-4, 114–116	200.68	AF	90	325.15	-44.38	R	1.21E-01	NA
26H-1, 32–34	201.21	AF	90	201.55	-37.31	R	9.62E-02	NA
27H-1, 104–106	211.43	AF	100	349.66	-44.91	R	7.53E-02	NA
27H-3, 75–77	213.735	AF	100	335.89	-58.31	R	1.54E-01	NA
28H-1, 10–12	219.99	AF	100	206.77	-21.84	R	1.42E-02	NA
28H-4, 17–19	222.09	AF	120	49.33	30.69	N	5.80E-03	NA
30X5, 26–28	238.56	TD	500	190.2	58.58	N	5.22E-05	NA
<b>316-C0008B-</b>								
1H-1, 126–128	1.26	AF	20–55	35.9	48.9	N	2.07E-03	19.2
1H-4, 104–106	5.275	AF	30–75	76.2	26.1	N	1.57E-03	6.7
1H-6, 91–93	6.79	AF	10–40	192.8	66.4	N	8.66E-03	16.2
<b>316-C0008C-</b>								
1H-3, 88–90	2.545	AF	20–75	166.3	66.4	N	1.09E-02	4.3
1H-3, 113–115	2.795	AF	15–75	92.2	60.8	N	2.95E-03	13
1H-4, 127–129	4.125	AF	15–55	101.4	55.2	N	4.08E-03	6.9
1H-6, 57–59	5.06	AF	30–75	184.2	47.1	N	7.18E-03	8.6
5H-2, 91–93	35.305	AF	8–15	81.7	60.9	N	1.60E-03	8.4
5H-4, 122–124	37.93	AF	30–75	52.6	-19.5	R	1.58E-03	18.9
5H-7, 117–119	40.465	AF	8–15	355.8	53.6	N	1.10E-03	15.7
5H-8, 102–104	41.62	AF	30–55	108.2	-13.2	R	1.15E-03	11.9
5H-10, 68–70	43.535	AF	30–55	50.4	-7.3	R	4.56E-03	8.9
6H-1, 123–125	44.74	AF	20–55	193.5	61.4	N	2.38E-03	8.2
6H-2, 138–140	46.19	AF	30–75	245.8	-16.5	R	1.72E-03	11
6H-3, 77–79	47.065	AF	30–55	262.3	-8	R	1.93E-03	10.6
6H-6, 125–127	50.305	AF	20–55	266.4	-45.1	R	1.77E-03	9.8
6H-7, 113–115	51.5	AF	40–75	280.9	-8.3	R	1.75E-03	2.2
7H-2, 77–79	54.43	AF	20–55	193.2	35.6	N	5.35E-03	10.5
7H-3, 64–66	55.6	AF	40–55	240.2	-19.1	R	2.40E-03	15.3
7H-6, 117–119	58.365	AF	55–75	288.1	-36.8	R	6.85E-03	11.6
7H-7, 101–103	59.515	AF	30–75	324.8	-13.7	R	9.66E-03	8.1
7H-8, 96–98	60.77	AF	40–75	242.2	-12.9	R	1.15E-02	14.3
9H-2, 64–66	69.24	AF	30–75	343.5	-63.3	R	1.66E-02	5.8
9H-3, 103–105	70.315	AF	30–55	326.6	61.8	N	1.00E-02	5.2
9H-6, 96–98	72.91	AF	20–40	322.1	61.9	N	1.11E-02	7.8
10H-1, 105–107	78.06	AF	20–30	158.7	-64.7	R	5.61E-03	8.4
10H-2, 98–100	78.3	AF	40–50	175.5	-21.8	R	1.64E-02	11.7
10H-4, 80–82	80.66	AF	20–55	208.6	-5.4	R	1.60E-03	6.4
10H-8, 113–115	83.235	AF	30–75	243.5	-6.1	R	1.17E-02	11.5
11H-3, 52–54	83.47	AF	30–55	302.5	-15.1	R	4.65E-03	9.7
11H-5, 43–45	84.65	AF	30–55	297.2	0.9	R	5.98E-03	10.6
11H-8, 109–111	86.535	AF	20–75	348	-48.6	R	1.88E-03	15.6
11H-11, 119–121	89.52	AF	30–55	3	-19.3	R	4.01E-03	2.4

**Table T1 (continued).**

Core, section, interval (cm)	Depth (mbsf)*	Demagnetization type	Range (mT/°C)	Declination (°)	Inclination (°)	Polarity	NRM intensity (A/m)	MAD (°)
11H-12, 95–97	90.82	AF	20–40	18.2	-17.2	R	4.78E-03	9
12H-1, 61–63	90.74	AF	40–75	302.8	-24.8	R	2.55E-03	8.8
13H-1, 79–81	92.05	AF	8–15	351.4	55.3	N	1.42E-02	0.6
13H-3, 36–38	92.15	AF	30–75	312.2	-18.7	R	3.76E-03	9
13H-5, 114–116	93.435	AF	40–75	353	-26.6	R	1.34E-02	0.7
13H-9, 77–79	95.87	AF	75	314.7	-39.2	R	1.80E-02	3.9
14H-3, 16–18	99.73	AF	20–40	69.6	26.9	N	2.00E-02	4.5
14H-9, 119–121	105.685	AF	55–75	94.2	52.3	N	5.22E-03	NA
14H-10, 8–10	105.885	AF	30–75	172.8	57.4	N	7.73E-03	5.8
14H-11, 44–46	107.055	AF	15–30	202.4	-22.8	R	3.36E-03	12.9
16H-2, 98–100	110.06	AF	40–75	173.3	-44.9	R	1.67E-01	3.1
16H-3, 42–44	110.73	AF	30–55	135.3	-26.8	R	5.61E-02	24.9
16H-6, 80–82	112.175	AF	30–40	126.6	-16.2	R	2.65E-02	4
16H-7, 106–108	114.72	AF	30–75	115	-29.9	R	4.85E-02	12
17H-3, 105–107	117.185	AF	20–40	156.3	61.6	N	2.71E-02	8.1
17H-4, 137–139	118.67	AF	20–75	331.3	43	N	5.32E-02	9.6
17H-5, 98–100	119.745	AF	10–30	38.6	37.9	N	1.45E-02	1.6
18H-2, 101–103	122.22	AF	55–75	227.5	-38.9	R	8.85E-02	10.9
18H-3, 113–115	123.665	AF	30–55	221	42.4	N	7.56E-02	6.7
18H-4, 77–79	124.615	AF	20–40	295.8	61.5	N	5.28E-02	11.4
18H-5, 95–97	126.115	AF	40–75	13.6	42.3	N	8.40E-02	24.9
19H-1, 77–79	126.16	AF	30–75	37.3	70.1	N	4.85E-02	12.3
19H-3, 15–17	126.97	AF	30–55	237.4	0.3	R	1.77E-02	19
19H-4, 54–56	127.875	AF	40–75	14.9	-3.8	R	1.98E-02	7.1

\* = Distances from core top, not depth. NRM = natural remanent magnetization, MAD = maximum angular deviation. AF = alternating-field demagnetization, TD = thermal demagnetization. N = normal, R = reversed. NA = not applicable.



**Table T2.** Summary of rock magnetic properties of Expedition 316 samples considered for this study.

Core, section, Interval (cm)	Depth (mbsf)*	Rock type	$T_c$ (°C)		$T_v$ (K)	$H_c$ (mT)	$H_{cr}/H_c$	$J_s$ ( $\mu\text{Am}^2/\text{kg}$ )	$J_r$ ( $\mu\text{Am}^2/\text{kg}$ )	$J_r/J_s$	
			[ $T_c1$ , $T_c2$ ] (Kappabridge)	[ $T_c1$ , $T_c2$ ] (MicroVSM)							
<b>316-C0004D-</b>											
27R-2, 35–37	266.76	Green-gray silty claystone				5.274	33.13	6.2817595753	1.422	0.0086	0.006
28R-3, 7–9	272.39	Green-gray silty claystone	390, 580		125?	10.09	73.45	7.2794846383	1.156	0.017	0.015
28R-3, 8–10	272.4	Green-gray silty claystone	310, 580								
29R-2, 11–13	275.505	Green-gray silty claystone				9.618	32.69	3.3988355167	1.501	0.02	0.014
30R-1, 124–126	279.74	Brecciated silty claystone	340, 575	368, 590	121	6.081	41.33	6.7965795099	0.605	0.003	0.0005
52R-2, 5–7	378.95	Olive-gray silty claystone	362, 595								
53R-2, 31–33	383.715	Olive-gray silty claystone	350, 550								
<b>316-C0006E-</b>											
17X-2, 24–26	99.98	Dark gray sandstone				2.115	37.03	17.5082742317	1.54	0.0039	0.002
34X-2, 66–68	260.4	Olive-gray silty claystone	570								
35X-1, 52–54	268.35	Dark olive silty claystone	379, 580			10.85	34.66	3.1944700461	8.555	0.717	0.08
39X-7, 36–38	313.245	Siltstone	590			7.164	24.99	3.4882747069	12.07	0.665	0.06
39X-8, 36–38	314.655	Olive-gray silty claystone	340, 580			24.8	34.1	1.375	2.31	7.53	0.307
40X-1, 28–30	315.61	Gray silty claystone	358, 585			7.946	22.47	2.8278379059	4.418	0.244	0.06
43X-7, 104–106	351.945	Green-gray claystone	325, 575								
44X-6, 24–26	359.61	Olive-gray silty claystone	357, 588		130	11.37	34.61	3.0439753738	5.435	0.559	0.1
44X-8, 76–78	362.59	Olive-gray silty claystone				11.51	23.93	2.0790616855	1.841	0.192	0.1
44X-cc, 11–13	362.995	Olive-gray silty claystone	370, 590			8.615	40.11	4.6558328497	4.96	0.279	0.056
<b>316-C0006F-</b>											
4R-1, 24–26	423.74	Greenish gray silty claystone	585								
12R-1, 127–129	496.27	Greenish gray silty claystone	290, 580								
16R-1, 32–34	533.32	Greenish gray silty claystone	370, 579			3.04	38.23	12.5756578947	0.657	0.027	0.004
17R-2, 24–26	544.115	Bioturbated silty claystone				2.115	37.03	17.5082742317	1.54	0.0039	0.002
23R-1, 64–66	594.14	Greenish gray silty claystone	400, 585								
<b>316-C0007C-</b>											
1H-3, 47–49	14.755	Dark gray sandstone	280, 550								
1H-6, 62–64	17.74	Green-gray silty claystone	582								
5X-cc, 5–7	43.24	Gray sandstone	170, 580								
9X-4, 55–57	85.855	Green-gray fine sandstone	310, 581								
14X-cc, 25–27	130.48	Olive-gray silty claystone	302, 575								
<b>316-C0007D-</b>											
15R-2, 25–27	305.155	Olive-gray silty claystone	330, 600		120	9.585	36.14	3.7704747001	5.043	0.396	0.078
24R-2, 126–128	391.67	Fine-grained sandstone	142, 580								
24R-4, 6–8	393.31	Fine-grained sandstone	140, 575								
25R-3, 48–50	401.845	Greenish gray silty claystone	160, 588								
29R-2, 86–88	438.765	Greenish gray silty claystone	119, 560								
<b>316-C0008C-</b>											
12H-1, 61–63	90.72	Silty claystone	583								

\* = Distances from core top, not depth. Rock types are from Expedition 316 visual core descriptions; see text for references.  $T_c$  = Curie temperature ( $T_c1$ ,  $T_c2$  = low and high Curie temperature, respectively).  $T_v$  = Verwey transition temperature. Hysteresis ratios are usually divided into regions: single domain (SD) for  $J_s/J_r > 0.5$  and  $H_{cr}/H_c < 1.5$ , multidomain (MD) for  $J_s/J_r < 0.05$  and  $H_{cr}/H_c > 4$ , and pseudosingle domain (PSD) in between (Dunlop, 2002).

